AN IMPLEMENTATION OF FUNCTIONALIZED CARBON NANOTUBES ON OPTICAL BIOSENSORS

by

Nalan Liv

Submitted to the Graduate School of Engineering and Natural Sciences
in partial fulfillment of
the requirements for the degree of Master of Science
in

SABANCI UNIVERSITY

Spring 2009

AN IMPLEMENTATION OF FUNCTIONALIZED CARBON NANOTUBES ON OPTICAL BIOSENSORS

APPROVED BY:

Prof. Dr. Hüveyda Başağa …….

(Thesis Supervisor)

Prof. Dr. Yaşar Gürbüz …….

Assoc. Prof. Uğur Sezerman …….

Assist. Prof. Javed Hussain Niazi Kolkar Mohammed …….

Assist. Prof. Nuri Solak …….

DATE OF APPROVAL: …….

AN IMPLEMENTATION OF FUNCTIONALIZED CARBON NANOTUBES ON OPTICAL BIOSENSORS

Nalan LIV

Biological Sciences and Bioengineering, M.Sc. Thesis, 2009

Thesis Supervisor: Prof. Dr. Hüveyda Başağa

Keywords

Functionalization of Carbon Nanotubes, Optical Biosensors, Antibody Array, Oligonucleotide Array

ABSTRACT

Carbon Nanotubes have attracted great attention since their discovery with their uniqueness based on outstanding mechanical, electronic and structural properties they have and wide application potential they promise. The significant properties of carbon nanotubes accumulated the studies on CNT-based electro analytical sensor applications. Although there is a huge amount of work on implementing CNTs for electrochemical studies, their implementation in optical biosensor platforms remains to be discovered.

Therefore, this study focuses on the Multi-Walled Carbon Nanotube implementation for optical biosensor platforms. The MWNTs were firstly functionalized via a two-step process of diimide-activated amidation and both the functionalized MWNTs and the protein immobilization on them were characterized with Dynamic Light Scattering, Fourier Transform Infrared Spectrometry and Scanning Electron Microscopy analysis. In order to explore the sensitivity enhancement that carbon nanotubes promise for immunosensor and oligonucleotide-sensor applications, microarray experiments in which functionalized MWNTs were used as a new microarray substrate were performed. MWNT coated slides enhanced the signal intensities of constructed platforms approximately 2 folds when antibodies were used as probe biomolecules with a lowest detection limit of 1,9 ng/ml. The signal enhancement served by the MWNT coted surfaces was 3 folds when oligonucleotides were used as probe biomolecules with a lowest detection limit of 1 nM. Also this MWNT coated slides and protein immobilization on them were further characterized via Scanning Electron Microscopy and Atomic Force Microscopy analysis.

The performed microarray experiments together with the other characterization studies, suggest functionalized MWNTs as good candidates for optical sensor platforms combining the benefits of increased surface area of 3D carbon nanotube structures, high binding capacity of MWNTs for biomolecules without changing their biologically active conformation, and the generation of a high signal to noise ratio according to the excellent low auto fluorescence of MWNTs.

.

OPTİK BİYOSENSÖRLERDE KARBON NANOTÜP UYGULAMASI

Nalan LİV

Biyoloji Bilimleri ve Biyomühendislik, Yüksek Lisans Tezi, 2009

Tez Danışmanı: Prof. Dr. Hüveyda Başağa

Anahtar Kelimeler

Karbon Nanotüplerin İşlevselleştirilmesi, Optik Biyosensörler, Antikor Arrayleri, Oligonükleotid Arrayleri.

ÖZET

Karbon Nanotüpler önemli mekanik, elektronik ve yapısal özelliklerinden kaynaklan eşsizlikleri ve gen,ş uygulama alanları sayesinde büyük ilgi toplamışlardır. Taşıdıkları bu önemli özellikler, özellikle son yıllarda karbon nanotüp temelli elektro analitik sensör çalışmalarının sayısının artmasını sağlamıştır. Her ne kadar karbon nanotüplerin elektrokimyasal sensör uygulamalarında kullanılması konusunda oldukça fazla çalışma olsa da, optik temelli biyosensör çalışmalarında kullanılmaları halen keşfedilmeyi beklemektedir.

Bu bağlamda, bu çalışma çok duvarlı karbon nanotüplerin optik biyosensör sistemleri için kullanılmasını içermektedir. Öncelikle, çok duvarlı karbon nanotüpler iki basamaklı bir amidasyon yöntemiyle işlevsellendirilmiş ve hem işlevsellendirilmiş çok duvarlı karbon nanotüler, hem de bu nanotüpler üzerinde yapılan protein immobilizasyonu DLS, FTIR ve SEM analizleri ile karakterize edilmiştir. Çok duvarlı karbon nanotüplerin optik antikor sensörleri ve oligonükleotid sensörleri için vaat ettikleri hassasiyet artırımını araştırmak için işlevsellendirilmiş nanotüp yapılarının substrat olarak kullanıldığı mikroarray deneyleri yapılmıştır. Yapılan bu deneylerde, nanotüpler ile kaplanan yüzeyler antikor arrayleri için sinyal seviyelerini yaklaşık iki kat, oligonücleotid arrayleri için ise yaklaşık üç kat arttırmıştır. Ayrıca, işlevsellendirilmiş çok duvarlı karbon nanotülerle hazırlanan bu yüzeyler ve bu yüzeyler üzerindeki protein immobilizasyonu SEM ve AFM metodları ile karakterize edilmiştir.

Yapılan mikroarray deneyleri ve diğer karakterizasyon çalışmaları işlevsellendirilmiş çok duvarlı karbon nanotüleri sundukları üç boyutlu yüzey, biyomolekülleri aktif konformasyonlarını kaybetmeden güçlü şekilde bağlayabilmeleri ve yüksek sinyal- parazit oranı sağlayan düşük oto-ışınımları sonucunda optik sensor platformları için güçlü adaylar olarak göstermektedir.

to my Mother

&

in the great memory of my Father

ACKNOWLEDGEMENTS

I would gratefully like to thank my supervisor Prof. Dr. Hüveyda Başağa for her guidance at all stages of my study and for everything I learned from her. I am also grateful to Prof. Dr. Yaşar Gürbüz and Assoc. Prof. Uğur Sezerman for their guidance, encouragement and support throughout my study.

I would like to thank Dr. Nuri Solak and Dr. Javed Mohammed for their precious contributions as jury members. I want to thank Dr. Nuri Solak once more for his help about the SEM analysis and for his kind encouragement.

Thanks to my friends for being always there for me: Evre, Merve, Gizem, Okşan, Arif, Dilek, İrem, Esra, Burcu, Naci, Evrim, Can…

I am especially thankful to Caner Hamarat & Hande Hazinedaroğlu for their love, motivation, care, friendship and support. I was very lucky to have them by my side for all these years at Sabancı University.

I am grateful to Özgür Gül for his help, support and encouragement. Thank you for being always there for me, for all ideas & information you shared with me, for your patience, and your time. Besides all these, I am also grateful to you for being such a great friend.

Last, but furthest, I want to thank my family, especially my mother who has always motivated and supported me throughout my whole life. I am deeply grateful to them for their endless love and care.

ABREVIATIONS

Ab	**Antibody**
Ag	**Antigen**
AFM	**Atomic Force Microscopy**
APTES	**3-aminopropyltriethoxy silane**
CNT	**Carbon Nanotube**
CRP	**C- reactive protein**
DLS	**Dynamic Light Scattering**
EDC	**1-ethyl-3-(3-dimethylaminopropyl) carbodiimide**
EIS	**Electrochemical Impedance Spectroscopy**
GCE	**Glassy Carbon Electrode**
ITU	**Istanbul Technical University**
MWNT	**Multi- Walled Carbon Nanotube**
NHS	***N*-hydroxysuccinimide**
PCR	**Polymerase Chain Reaction**
SAM	**Self Assembled Monolayer**
SNP	**Single- nucleotide Polymorphism**
SSB	**Single Strand Binding Protein**
ss-DNA	**Single Stranded DNA**
SWNT	**Single- Walled Carbon Nanotube**
STREP	**Streptavidin**

TABLE OF CONTENTS

LIST OF TABLES

LIST OF FIGURES

I. INTRODUCTION

1.1 BIOSENSORS

A biosensor is an analytical device that recognizes the presence of the species of interest and converts it into an electrical signal. A biosensor must include typically three major parts which are the target; the biosensing probe, which is able to recognize the target; and the transducer which will convert the presence of the target into an electrochemical signal. Application area of biosensors is really wide and some examples can be food and agricultural product safety, medical diagnostics, military applications as chemical and biological agent detection, etc. Biosensors emerge as promising tools for both laboratory and in-field applications. The first biosensor, a glucose sensor was developed by Clark and Lyons in 1962 **[1].**

1.1.1 Classification of Biosensors

Classification of biosensors can be made according to either the biosensing element or the transducer. According to the biosensing element, there are three types of biosensors; first one is *biocatalysis-based biosensors*, which use enzymes as their biosensing elements; second is *cell-based biosensors*, which use whole-cells or microorganisms as biosensing elements; and the last one is *bioaffinity-based biosensors,* which compose the focus of this research and will be mentioned in more detail. *Bioaffinity-based biosensors* use either antibodies or oligonucleotides as their sensing elements. The ones involving antibodies, so called *immunosensors*, the mechanism of action is based on the specific interaction between an antibody and its antigen. And the ones involving nucleotide structures as the biosensing element, so called *oligonucleotide- sensors* or *dna-sensors*, the mechanism is based on the specific interaction between the oligonucleotide strand and its complementary strand. Although they are more complex than the other biosensing systems, they promise more selectivity and more specificity.

According to the transducer type, biosensors can be classified in four different groups.

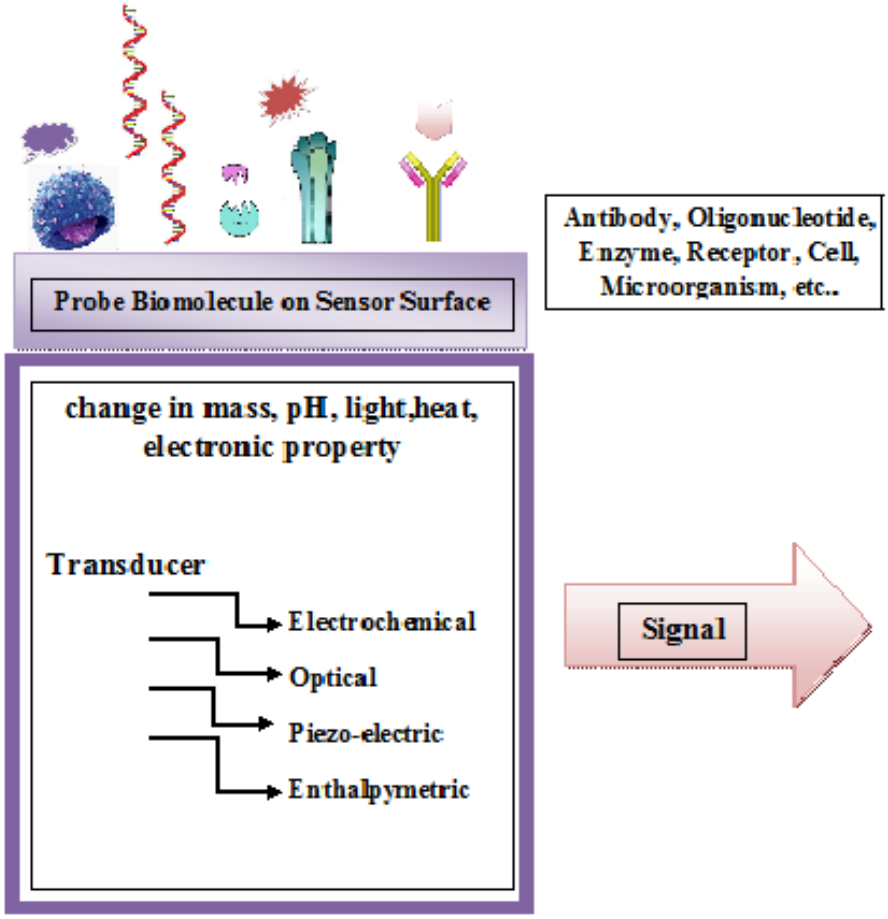

Fig 1.1. Schematic & Classification of Biosensor Systems.

1.1.1.1 Electrochemical Transducers

Electrochemical Transducers use a chemical change as the input parameter, and outputs it as an electrical signal which must proportional to the input. There are many different examples of electrochemical transducers, and most commonly used ones are described below.

The sensors which are based on the measurement of the potential difference between the working electrode and the reference electrode are called *Potentiometric Sensors*. A logarithmic relation bared by the target analyte is used to calculate the generated potential. Although these transducers promise a wide detection limit, their requirement for a very stable reference electrode limits their usage. *Amperometric sensors* are based on the detection of the current change due to the oxidation or reduction at the working electrode. The output is generated with the linear proportion between the generated current and the concentration of the present analyte. Like in the

potentiometric transducers, the requirement for a stable reference electrode sets a barrier to their usability. Another example for electrochemical transducers can be *Conductometric sensors,* which generate the output from a logarithmic function derived from the change in the ionic strength of the working electrode have similar advantages and disadvantages with other electrochemical detection systems **[2]**.

1.1.1.2 Piezo-electric Transducers

These biosensors are composed of microbalances based on piezoelectric crystals, where a decrease of the resonance frequency is correlated to the mass accumulated on its surface. These crystals are referred as quartz crystal microbalances (QCM). The potential of piezoelectric devices for chemical sensor applications was realized by Sauerbrey **[3],** who derived the following equation describing the frequency-to-mass relationship:

$$\Delta f = \frac{-2\Delta m f_0^2}{A\sqrt{\rho_q \mu_q}} = -\frac{2f_0^2}{A\ \rho_q v_q}\Delta m$$

The equation clearly indicates that the oscillating frequency is linearly dependent on the change in mass of adsorbed material at the crystal surface. To give some examples of these sensors, surface flexure plate wave (FPW), acoustic wave (SAW), shear horizontal surface acoustic wave (SH-SAW), thickness shear mode (TSM) sensors can be listed.

1.1.1.3 Enthalpymetric Transducers

These sensors are based on the measurement of generated heat change which is directly related with the concentration of the present analyte on the sensor surface. Therefore, enthalpymetric sensors are also referred as calorimetric or thermal biosensors **[4]**.

1.1.1.4 Optical Transducers

Optical sensor systems have been the oldest and the most widely used transducers for biosensor platforms. Optical transducers can use several types of detection methods, but the common property of each is that the transduced signal will be generated from light. For example, *Absorption Transducers* measure of intensity of absorbed or reflected light on the sensor platform, the principle of these systems is based on the Lambert-Beer law, which indicates a linear proportion between the

concentration of the analyte present and the measured absorbance. As another example, *Luminescence Sensors* measure the luminescence response upon UV excitation. These sensors can detect mainly two types of luminescence, first one is bioluminescence which will be generated by a living organism and the other one is chemiluminescence which will be generated by a chemical reaction. One other example, *Fluorescence Sensors* involves the measurement of fluorescence response upon excitation. And the last example, *Surface Plasmon Resonance (SPR)* technique is based on the measurement of the change in the refractive index of the sensor surface generated when the target molecules bind to the surface **[5]**.

1.1.2 Challenges in Biosensor Technologies

There are five key steps in biosensor development. Firstly, the architecture of the planned sensor must be designed and constructed as one of the transducer types mentioned below. Fabrication method which can be either screen printing or microfabrication is the second step. The third step consists of the decision of the material that will be used as the probe or in other words as the biosensing element. After the probe is decided, method of immobilization must be determined, which can include adsorption, entrapment, microencapsulation, covalent attachment, etc. The last step is signal processing **[6].**

The developed biosensor systems must satisfy several criteria as sensitivity and specificity, potential for continuous monitoring, rapidity in response, inexpensive production, user-friendly, stability and reproducibility, easy to manufacture, compactness, etc. In spite of the past and current large amount of research in biosensor development, there is still a challenge to create improved and more reliable devices. There are many completed and still going- on research studies exist to improve either one or some of the criteria mentioned above. General improvement strategies are tried to be classified and explained with their key considerations below.

Firstly, there is a growing tendency toward *miniaturization* of analytical systems, since it reduces the reagent consumption, allows the easy handling of samples with lower volumes, and increases sample throughput **[7]**. Miniaturization can create less expensive, easy to handle devices, which will be especially important for in- field analysis.

Production of inexpensive sensors not only needs miniaturization, but also requires *batch-fabrication*. Automated manufacturing technologies are required for the commercial production of large numbers of inexpensive, reproducible biosensor devices **[8]**. The need of clinical markets for large biosensor amounts can only be enabled with mass fabrication methods.

Lastly, the state- of-art technologies include improving bio-sensing interfaces, design and analysis on the molecular level. All are addressing bio-interfaces in molecular dimensions and thus can be summarized by the term *"molecular nanotechnology"* **[9]**. Therefore, there is a trend toward the combination of physics and biology in the creation of new nanostructures. Nanotechnology comprises a group of emerging techniques from physics, chemistry, biology, engineering, and microelectronics that are capable of manipulating matter at nanoscale. Nanotechnology promises to bridge the gap between materials science, coming from the micrometer range, and biochemistry- chemistry, where individual molecules are of the major interest **[10]**.

1.2 MICRO-ARRAY TECHNOLOGIES

Both for DNA and proteins, microarrays provide a powerful analytical tool for the simultaneous analyses of thousands of parameters in a single experiment. As described in Ekins *et al.*, microarray technologies was first applied for immunological ligand-binding assays and quickly draw attention with the improved sensitivity and high- throughput results that it provides compared to other techniques **[11].** Microarray techniques are then widely used for DNA as diagnostic tools, aiming mostly to identify gene expression levels and single nucleotide polymorphisms (SNPs) **[12, 13].** Also, micro-array based assays are used to characterize the proteome **[14, 15].** Both protein and DNA based micro-arrays find application in wide areas like medical applications to toxicology studies. They are also able to provide information about the response of a cell to a specific substrate or even profiling the protein expression differences in a cell caused by a specific condition of interest. Furthermore, with the developed living cell micro-arrays, their usage provides information about the interaction of live cells with the interested biomolecules. **[16, 17]**

Microarrays are produced with the immobilization of high density biologically proper probes as discrete arranged spots. A microarray can serve up to 10^7 spot sites in

$100mm^2$ areas ready for testing **[18].** The DNA, protein, oligonucleotide or carbohydrate samples which will be used as the probe molecules are immobilized on a solid surface in a patterned manner by using spotting, contact printing or photolithography. The immobilized molecules are then become ready to capture the target molecules through specific interactions. The detection principle can vary, but many of the commercially available microarrays make use of fluorescent labels and fluorescent detection, through existing alternative labeling strategies as well as label-free detection methods are also being developed. And finally, the acquired data is analyzed with the help of bioinformatics tools.

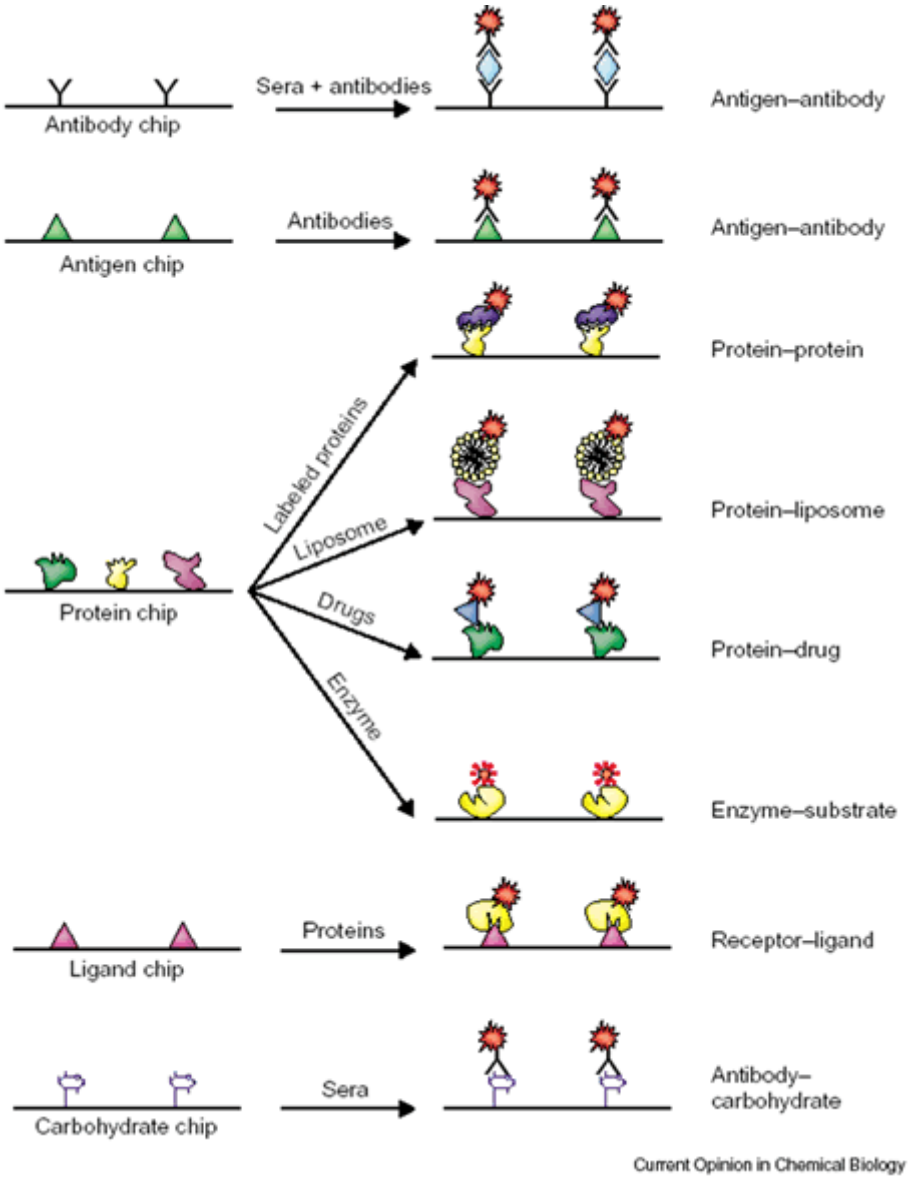

Fig 1.2. Applications of Protein Microarrays **[88].**

1.2.1 DNA Micro-arrays

In spotted DNA micro-arrays, the immobilized probes can be small PCR product fragments, cDNA, oligonucleotides. Each of the probes will have a different sequence structure which will specifically recognize the sequence of interest. DNA micro-arrays are formed with spotting these probes onto the microarray substrate in an array format. Once the probes are spotted on the surface, they become ready for further hybridization with their complementary cDNA or cRNA targets derived from medical or experimental samples. These arrays can be adapted or customized to different experiments easily, because it allows the researchers to manipulate the set of chosen probes and printed array locations for each probe. They can also synthesize the probes themselves; label their own target sequences for hybridization. If the researchers have appropriate equipment, they can even print and scan the arrays themselves. This provides a relatively low cost analysis compared to other techniques and some commercially available arrays **[19].** Application area of DNA micro-arrays is really wide, covering gene expression analysis, comparative genomic hybridization, chromatin immunoprecipitation, SNP detection, alternative splicing analysis, etc.

1.2.2 Antibody Micro-arrays

As mentioned above, microarray technology and genomics serves opportunities to analyze a huge number of oligonucleotide samples in a single experiment and investigate the expression change of interested mRNA products in the cell in a specific condition. Although this is a really important analysis, the mRNA expression in a cell does not always correlate with the expression level of the protein that this specific mRNA is responsible for. This concept calls for the need of protein arrays, to be able to analyze protein expression change in a cell as a response to the interested specific conditions **[20].** The most common type of these mentioned analytical protein arrays are antibody microarrays in which antibodies that bind specific antigens are arrayed on a glass slide at high density like in DNA-array experiments. Then a lysate is passed over the prepared array and the bound antigen is detected after washing steps.

1.2.3 State of Art: Problems & Achievements

Micro-array technologies have captured great attention with their high-throughput results and distinct opportunities that they serve for analyzing very high numbers of protein–protein or compound–protein interactions simultaneously with a high dynamic range and low detection limits. However, their high-throughput capability

is directly dependent on the ability to immobilize a certain number of spots with different receptors on a limited area. For supplying high spot densities, piezo-electric, ring and pin arrayers serve technological solutions. Just like in the case of affinity biosensors, more important concept seems to be the design of the micro-array surface which has to attain some requirements like, high immobilization density of receptors, adequacy of keeping immobilized biomolecules in an active state, adequacy of inhibiting nonspecific adsorption, adequacy of limiting matrix effects of complex biological solutions on the qualitative and quantitative specific detection of interested target.

In the beginning of array fabrication, firstly the probes must be attached to a solid surface which must have maximum binding capacity for the indented probe. The probes, either oligonucleotides or proteins, immobilized on the surface with a attachment substrate layer. This layer can vary corresponding to different types of probes and applications. A huge variety of materials are studied and being studied including porous polyacrylamide hydrogels, other hydrogel- like hydrophilic polymers, polyaminoacids **[21]**, dextran-based hydrogel **[22],** and agarose **[23].** A practical method for attachment of the probes is using nitrocellulose-membrane or poly-L-Lysine coated glass, on which probes can be passively immobilized on the surface through non specific interactions **[24, 25, and 26]**. The disadvantages of these methods are the random immobilization of the probes to the surface and high noise to signal ratio because of the non- specific interactions. Suggesting a more stronger and specific immobilization, glass substrates with reactive chemical groups is a more suitable method for probe immobilization in micro-array technologies. These chemical groups interact with the chemical groups on the probe and covalently cross-link the probes on the surface **[27, 28]**. Usually a bifunctional silane chemical cross-linker is used to form a SAM on the surface. This silane bind to the hydroxyl groups on glass and another group stays free to react with primary amine groups of the interested probes or it can also be further modified to have maximum specificity for the interested probes **[29, 30]**.

This research proposes Multi-wall Carbon Nanotubes as surfaces for biosensor platforms and investigates their characteristics as micro-array substrates. Carbon Nanotubes are unique structures and they have attracted great attention since their discovery. Their uniqueness bases on their outstanding mechanical, electronic and structural properties. Their application potential covers a wide range from electronics,

microscopy, and composite materials to chemical and biological sensing. Most of these applications are close to experimental realization. However, acquired pristine carbon nanotubes are far away from being able to implement on the mentioned application areas. They need further chemical functionalizations to get involved in application plans. The functionalization of carbon nanotubes is a hot research topic as different chemical functionalizations of the nanotubes extends the scope of their application spectrum.

1.3 CARBON NANOTUBES

1.3.1 Structure of Carbon Nanotubes

Carbon nanotubes (CNTs) which can be described as cylindrical molecules or chemical structures are formed by rolled up graphite sheets of hexagonal carbon that are capped by pentagonal carbon rings. Carbon has the ground state configuration of $2s^2$, $2p^2$ with having four electrons in its outer valence shell. Three types of hybridizations are possible to occur in carbon: sp, sp^2 and sp^3. Diamond and graphite, two natural crystalline forms of pure carbon have sp^3 and sp^2 hybridizations, respectively. Carbon nanotubes have dominant sp2 and a small amount of sp3 hybridized carbon atoms **[31].** Therefore, CNTs have two types of bonds. Along the cylinder wall, the in-plane σ bonds form the hexagonal network. The out-of-plane π-bonds are responsible for the weak van der Waals interaction between the layers in MWCNTs, and between MWCNTs or SWCNTs in the bundles. However, curvature produces a local strain in the π–ring systems **[32].**

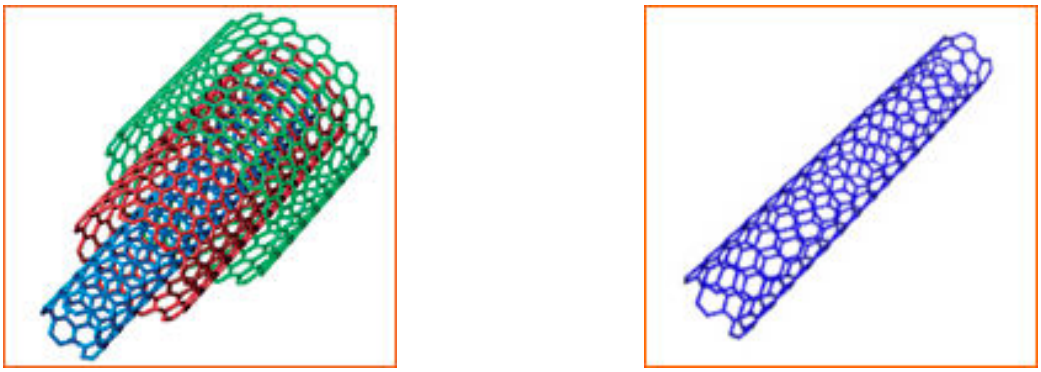

Fig 1.3. Multi- walled & Single- walled Carbon Nanotubes, respectively.

There are mainly two types of carbon tubes: Single-walled carbon nanotubes (SWCNTs) and Multi-walled carbon nanotubes (MWCNTs). SWCNTs are rolled up

from a single graphene sheet where the wall of the resultant nanotube is a single layer with closed ends. The nanotubes are classified as either having a zigzag, armchair or a chiral structure depending on the manner the graphene sheet is rolled up. SWCNTs have diameters of typically 1 nm with the smallest diameter reported to date being 0.4 nm. MWCNTs are a stack of graphene sheets rolled up into concentric cylinders with a layer spacing of 0.3-0.4 nm. MWCNTs tend to have diameters in the range 2-100 nm **[33].** The unique structure of CNTs leads to a number of unusual properties in these materials. MWCNTs are regarded as metallic conductors **[34].** SWCNTs are a mixture of metallic and semiconducting material, depending sensitively on their geometrical structures **[35].**

1.3.2 Production & Purification

Methods such as electric arc discharge, which involves the growth of CNTs on carbon (graphite) electrodes during the direct current arc-discharge evaporation of carbon in the presence of an inert gas such as helium or argon, laser vaporization in which a piece of graphite target is vaporized by laser irradiation under high temperature in an inert atmosphere and chemical vapor deposition techniques are well established and most widely used to produce the wide variety of MWCNTs.

Electric arc discharge, which involves the growth of CNTs on carbon (graphite) electrodes during the direct current arc-discharge evaporation of carbon in the presence of an inert gas such as helium or argon **[36],** is the easiest and most common method of producing CNTs. In Laser Vaporization Method, a piece of graphite target is vaporized by laser irradiation under high temperature in an inert atmosphere. MWNTs were found when a pure graphite target was used **[37].** Other widely used method, chemical vapor decomposition (CVD), has been used for many years to produce carbon fibers. Therefore, it is a well- known and a more optimized production technique when compared to other widely used techniques. CVD involves the decomposition of a hydrocarbon in the presence of a catalyst and was first used in 1993 by Yacaman *et al*. & in 1994 by Ivanov *et al*. & Amelinckx *et al*. to produce MWCNTs **[38, 39 and 40]**.

As-synthesized CNTs prepared by the above methods inevitably contain carbonaceous impurities and metal catalyst particles, and the amount of the impurities commonly increases with the decrease of CNT diameter. To fulfill the vast potential applications and to investigate the fundamental physical and chemical properties of

CNTs, highly efficient purification of the as-prepared CNTs is, therefore becomes an important concept. Purification methods involve different chemical and physical methods which will not be discussed further here **[41]**.

1.3.3 Properties of Carbon Nanotubes

Depending on the crystal structure of the graphene sheets, CNTs can be metallic or semiconducting. The electronic transport occurs directly in metallic nanotubes. This allows the nanotubes to conduct electricity with minimal resistance **[42]**. For example in copper, the maximum current conductivity is 59.6×10^6 S/m **[43].** Bulk MWNTs produced by arc discharge method have the conductivity ~ 100 S/cm , or 10^4 S/m **[44],** annealed multi-walled nanotubes, produced by chemical vapor deposition method have the conductivity 2×10^5 S/m **[45]**. High mechanical and chemical stability of carbon nanotubes is also a promising and outstanding property that CNTs serve. In terms of tensile strength and elastic modulus, carbon nanotubes are one of the strongest materials yet discovered; tensile strength of a typical SWNT is 56 times that of a steel wire and 1.7 times that of silicon carbide nanorods **[46]**.

Table 1.1. Evaluated properties of carbon nanotubes [35]

Property	Evaluation
Maximal supported electrical current density	~100 times greater than for copper wires
Thermal conductivity	>diamond
Tensile strength	~100 times the strength of steel
Young's modulus	stiffer than any other material
Carrier mobility	>hole mobility in Si

Also, corresponding to their size and chemical composition, properties of carbon nanotubes offers them to be used in medical and biological studies. The physical interaction between nanotubes and bacterial cell walls promises the potential use of

carbon nanotubes in microbiology studies **[47]**. Nanotubes can also penetrate the lipid bilayer of microbial cells, and allow release of intracellular contents through the artificial pore **[48]**. To focus on the subject of this study, the remarkable sensitivity that CNT conductivity brings in the surface proposes the use of CNT as highly sensitive nanoscale sensors. These properties make CNT extremely attractive for a wide range of electrochemical biosensors ranging from amperometric enzyme electrodes to DNA-biosensors.

1.3.4 Functionalization of Carbon Nanotubes

Carbon nanotubes have attracted great attention because of their unique structural, electronic, mechanical and thermal properties. The incorporation of CNTs into different chemical, electrical and biological systems will surely enhance the thermal and mechanical properties of these systems **[49].** However, the realization of nanotube-reinforced systems can only be achieved by solving following main problems. The atomically smooth nonreactive surface of nanotubes that is built of rolled graphene sheets and the poor dispersion of nanotubes in the many solvents limit the potential utilization of carbon nanotubes in many application areas **[50].** In addition to that, because of the fine size and high surface energy of CNTs, with intrinsic van der Waals forces, bare CNTs were apt to aggregate and entangle together spontaneously. These problems can be overcome by using different functionalization methods for carbon nanotubes which can provide multiple bonding sites to the organic/ inorganic reactants **[51].** The dispersion and solubility of CNTs in a solvent depends on the type and concentration of the functional chemical groups or molecules adsorbed on the tube surface. In this study, a covalent functionalization approach is used, therefore more information about covalent functionalization of CNTs will be provided.

The covalent functionalization of CNTs allows functional groups to be attached to tube end or side walls. Dissolution of CNTs in organic solvents requires the introduction of a hydrophobic substituent onto the carboxylic groups. Functionalization with different amines has been widely investigated to obtaining soluble CNTs, via covalent bonds **[52-54],** ionic bonds **[53, 55, and 56]** and physisorbed amines **[57, 58].** The first report to form soluble SWCNTs using octadecylamine (ODA) was made by Chen *et al* **[59].** They found that the functionalized tubes are soluble in a variety of organic solvents, such as chloroform, dichloromethane, benzene, chlorobenzene, 1,2-dichlorobenzene, and carbon disulfide. Further studies showed that direct thermal

mixing of oxidized SWCNTs and alkylamines forms ion pairs **[53]**, which are soluble in common organic solvents.

This ionic bond can be changed by introducing other organic and inorganic cations. Electrostatic interactions between CNTs and biological molecules are then possible, and these can serve as the basis for developing biocompatible CNTs. SWCNTs functionalized by esterification with pentanol enable the tubes to dissolve into some organic solvents **[60].** The photochemical behavior of soluble alkyl ester-modified nanotubes gave rise to measurable photocurrents after illuminating solutions of these tubes. As well, the transient spectrum of the charge separated state was detected **[61].**

1.3.5 Applications of Functionalized Carbon Nanotubes

The modification of CNTs has attracted considerable attention over the past decade so, with several hundreds of papers published on the subject; the methods and substrates used to modify CNTs appears to be almost solely limited by the imagination of the scientists.

The applications of functionalized CNTs are increasing with the use of promising structural and physicochemical properties of modified CNTs, which can be grouped as electrochemical applications of modified CNTs for electroanalysis **[62]**, bioelectroanalysis, **[63]** and the applications of modified CNTs for biomedical **[64]** and other bioanalytical applications **[65].** Carbon nanotubes can be utilized within widespread applications, such as molecular electronics, transportation of drugs and genes, preparation of blends with polymers, electroluminescent devices, even as scaffolds for cell growth. For example, embedding carbon nanotubes in polymeric matrices for various nanocomposite materials has been a popular subject in the nanotube research **[66, 67]**. Results from the experimental preparation and fabrication of polymeric carbon nanocomposites based on pristine carbon nanotubes suggest that the dispersion of the nanotubes in polymer matrices is a challenging task. This is a particularly serious issue for nanocomposites that are designed for optical applications because the aggregation of carbon nanotubes, among other problems, reduces the optical quality of the composite materials.

To focus on an application area, the significant potential biological applications of carbon nanotubes have already attracted much attention. For example, Tsang et. al. reported the immobilization of oligonucleotides and many other studies reported the

immobilization of enzymes, and proteins on MWNTs **[68]**. Balavoine and co-workers used MWNTs for helical crystallization of proteins to take advantage of their shape and exceptional rigidity **[69]**. Mattson, Haddon, and co-workers also reported on the growth of embryonic rat-brain neurons on MWNTs **[70]**. The biocompatibility of carbon nanotubes is a significant issue in many of their proposed bio-applications. For the preparation of nanotube- protein bioconjugates, specifically, the different salvation and other requirements for the handling of bioactive molecules and for the processing of carbon nanotubes represent significant challenges **[71]**.

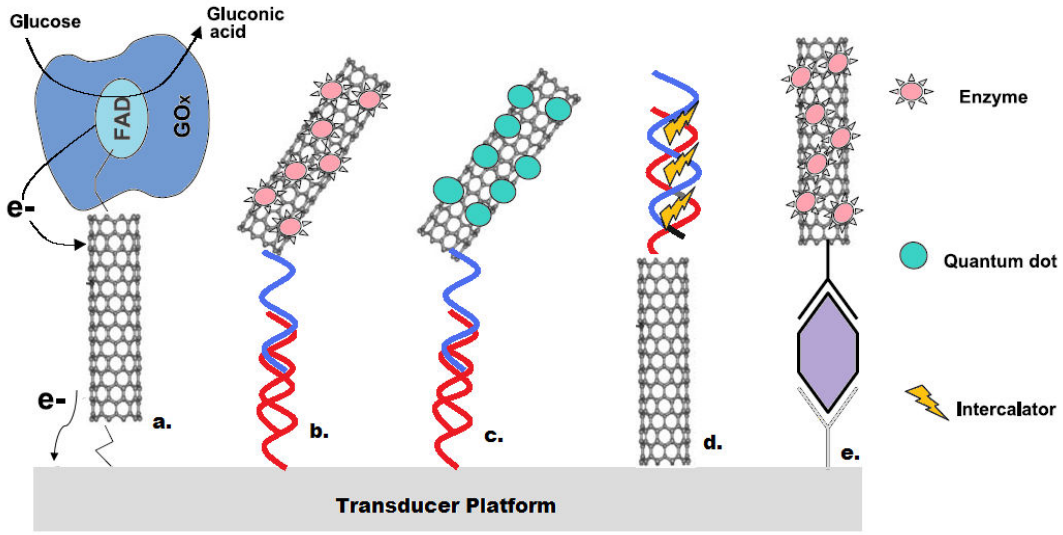

Fig 1.4. Applied Strategies Involving CNTs in Sensor Instrumentation **[89].**

Many other recent studies report about the electrochemical reactivity enhancement which carbon nanotubes provide to important biomolecules **[72, 73]**. This makes CNTs excellent candidates for electrochemical sensor implementations. In addition to this electrochemical reactivity enhancement, CNT-modified electrodes have been shown successful in accumulating important biomolecules **[74]** and alleviating surface fouling effects which promise for the potential use of CNTs not only in electrochemical but also in optical sensor instrumentations.

1.4 CNT-BASED IMMUNOSENSOR & DNA-SENSOR STUDIES

Although there is a huge amount of work on CNT- based enzyme sensors, they have been less widely used for the design of affinity biosensors. Interesting examples about CNT-based DNA-sensors and immunosensors will be mentioned below.

Recently, a label-free immunosensor for total prostate-specific antigen (T-PSA) using SWCNTs-array-modified Pt microelectrodes has been reported. The interaction between the T-PSA antigen and the T-PSA monoclonal antibody which is covalently immobilized on SWCNTs increase the oxidation of tyrosine and tryptophan residues, and the constructed sensor detects this enhanced oxidation. The detection limit for T-PSA was enhanced with the use of SWNTs on the electrode **[75]**. Another example reports an amperometric immunosensor for the detection of carcinoembryonic antigen (CEA) which is constructed with layer-by-layer assembly of gold nanoparticles–MWCNTs-thionine–Chit multilayer films on SAM-modified gold electrodes **[76]**.

One other example presents an electrochemical immunosensor for cholera toxin (CT) using poly(3,4-ethylenedioxythiophene)- coated CNTs and liposomes. Detection of CT is achieved with the labels which include ganglioside (GM1)-functionalized and potassium ferrocyanide encapsulated liposomes. The probe responsible for capturing CT was a monoclonal antibody against the β-subunit of CT which is also linked to poly (3,4-ethylenedioxythiophene) coated MWCNTs on a GCE. The experimental set-up was consisted of a sandwich-type assay, where the toxin is first bound to the anti-CT antibody and then to the GM1-functionalized liposome which then leads to electrochemical oxidation of potassium ferrocyanide. The oxidation was then measured by square wave voltammetry **[77]**. One of the recent works suggest a covalently bound anti-biotin antibodies embedded into a polylysine (PLL)-SWCNT composite layer coupled with an amperometric transducer. The system composed of covalently linked PLL, SWNTs and anti-biotin antibodies on the surface which enables both the enhanced detection of HRP labelled biotin and the enhanced thermal stability of the sensor **[78]**. Finally, as a last example, Yun *et.al* used EIS and cyclic voltammetry for characterization of antigen binding to anti-mouse IgG which is covalently immobilized on CNTs.and to measure different concentrations **[79]**.

Concerning DNA-sensor development with the use of CNTs, for the electrocatalytic oxidation of guanine, β-cyclodextrin-incorporated CNTs-modified electrodes have proved their usefulness, which make very low detection limits like 10 ng/ml DNA possible **[80]**. An example, an electrochemical sensor design showed the catalytic ability of MWCNTs for the direct electrochemical oxidation of guanine or adenine residues of ssDNA and adenine residues of RNA, leading to indicator-free detection of ssDNA and RNA. Proposed method can be used in detecting calf thymus

ssDNA in 5 minutes of hybridization time **[81]**. Another example makes use of binding event between *Escherichia coli* single strand binding protein (SSB) and ss-DNA causing an intrinsic oxidation of guanine residues. The system consists of ss-oligonucleotides immobilized on a SWNT modified electrode which causes a decreased voltametric signal when it binds to SSB **[82]**. Also, use of MWCNTs-modified graphite pencil electrodes in DNA– sensors is presented in which the system is based on the enhancement of guanine signal using differential pulse voltammetry **[83]**.

To detect salmon sperm DNA, CNTs onto graphite electrodes were used. The constructed system reached a detection limit of 0.252nM for double-stranded salmon sperm DNA with the enhancements in electro active surface and heterogeneous electron transfer provided by the CNTs on the surface **[84]**. Also, a DNA-sensor which is able to detect complementary sequence at 5.0×10^{-6} μM was reported. The sensor was prepared with MWCNTs as GCE modifiers **[85]**. Another study showed the detection of complementary DNA strand with DNA probe immobilized on paste electrode assembled by MWCNTs. The sensor detects the current change appears with the hybridization to the complementary sequence in which oxidation peak current was linearly related to the logarithm of the concentration of the complementary DNA sequence **[86]**. As a last example, a sensitivity enhanced DNA-biosensor was constructed by using palladium nanoparticles in combination with MWNTs which are dispersed in nafion. This combination was used to modify GCE, on which probe oligonucleotides were covalently attached to the carboxylic groups of MWCNT **[87]**.

2. AIM of THIS STUDY

Biosensors allow the detection of defined biomolecules simultaneously with high dynamic range and low detection limits. Especially for the optical biosensor systems, high-throughput capability is directly dependent on the ability to immobilize a certain number of probes (biomolecules) on a limited area. In this aspect, designing the biosensor surface, which has to attain some requirements such as high immobilization density of probes, adequacy of keeping immobilized biomolecules in an active state, adequacy of inhibiting nonspecific adsorption, adequacy of limiting matrix effects of complex biological solutions, containing the biomolecule of interest is crucial.

This study aims to implement functionalized MWNTs as new surfaces for optical biosensor applications. Although there is a huge amount of work based on the electrochemical studies including CNTs, their implementation on optical biosensors remains to be discovered. Besides the electro catalytic ability of CNTs-modified electrodes, their enhanced active surface area and the anti-fouling capability of the modified surfaces promise enhancement effects on optical systems, which this study aims to discover. High binding capacity of MWNTs for biomolecules without changing their biologically active conformation is presented as well as a low auto fluorescence which is very important in order to generate a high signal to noise ratio in optical sensor systems are studied. Microarray experiments present MWNTs as good candidates for optical sensor platforms combining the benefits of increased surface area of 3D carbon nanotube structures with the excellent low auto fluorescence of carbon nanotubes as a black substrate.

3. MATERIALS & EXPERIMENTAL

3.1 Reagents

MWNTs (Baytubes®) with purity > 95%, length 1-5 μm and diameter 30±10 nm which are synthesized by CVD were obtained as a free sample from Bayer MaterialScience (Leverkusen, Germany) and used without further purification. Carboxy and Hydroxy functionalized MWNTs with purity > 95%, length 4-5 μm and diameter 20 nm were purchased from Arry Nano materials and Nanotechnology (Hong Kong, China). 1-ethyl-3-(3-dimethylaminopropyl) carbodiimide (EDC) and 3-aminopropyltriethoxy silane (APTES) were from Sigma-Aldrich. *N*-hydroxysuccinimide (NHS) was obtained from Aldrich. All other reagents and chemicals were of analytical grade and obtained from Sigma–Aldrich (St. Louis, MO). Water used for preparation of aqueous solutions was from a Millipore Direct-Q Water system (resistivity, 18 MΩ cm^{-2}). All chemicals and reagents were used as-received without further purification.

3.2 Functionalization of Carbon Nanotubes

3.2.1 Carboxyl Functionalization of Baytubes®

A suspension of 10 mg of Baytubes® was sonicated in a sonicator bath at room temperature for 12 hours in a 40 ml mixture of 3:1 (v/v) 98% H_2SO_4 and 70% HNO_3. The contents were allowed to cool and sufficient time was given to let the nanotubes to settle down. The supernatant was discarded and the filtrate was extensively washed with de-ionized water and filtered by centrifugation until the pH of the solution was 7. The filtrate was then freeze dried and a dark solid product of MWNT-COOH was obtained.

3.2.2 Functionalization of CNTs with EDC/NHS

8 mg of freshly oxidized MWNTs were suspended in 5 mL of deionized water by sonicating the mixture for 2 hours with a sonicator tip. Then, 1 mL of 500 mM MES buffer solution, pH 6.1 and 2.3 ml of a 50 mg/mL aqueous solution of NHS were added to the above suspension. Under fast stirring, 1.2 mL of freshly prepared 10 mg/mL aqueous solution of EDC was, and the mixture was stirred continually at room temperature for 2 hours. The suspension was filtered by centrifugation several to remove excess EDC, NHS and the by-product urea. If they will not be directly used for

protein immobilization, the filtrate was re-suspended in 10ml ddH_2O and labelled as *8X_MWNT_NHS*.

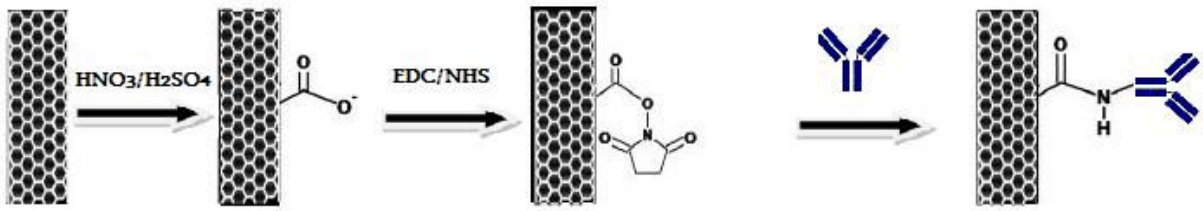

Fig 3.1. Covalent Immobilization of Antibodies on MWNT surface.

3.2.3 Functionalization of CNTs with APTES

8 mg of oxidized MWNT were suspended in 10% APTES by heating the solution to 60°C for 6 hours followed by stirring at room temperature for 3 hours. APTES modified MWNTs were recovered by centrifugation and rinsed thoroughly with water.

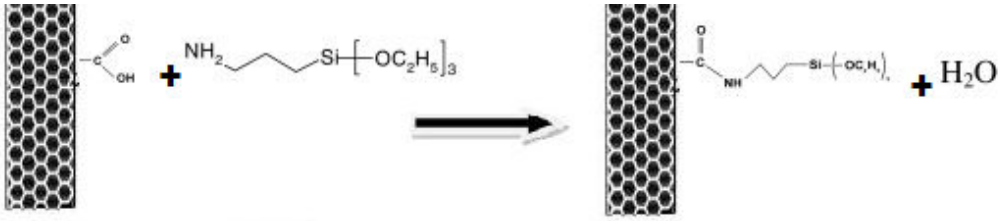

Fig 3.2. Functionalization of CNTs with APTES.

3.3 Protein Immobilization on Carbon Nanotubes

The activated CNTs were then re-dispersed in 9 mL of ddH_2O, and 1 mL of a 0.2 mg/mL CRP_Cap_Ab in PBS. After incubating the mixture on a platform shaker at 4°C for 12 hours, the nanotube suspension was centrifuged at 13200 rpm and rinsed several times with water to remove any unbound protein. The protein- nanotube conjugate was finally suspended in 10ml ddH_2O. A part of the sample was freeze dried for characterization studies.

3.4 Characterization of Functionalized & Protein Immobilized Carbon Nanotubes

3.4.1 Scanning Electron Microscopy (SEM)

Samples of functionalized and protein immobilized CNTs in solution were prepared by dropping a small amount of CNT solution on the sample holder and

allowed to air dry overnight. The samples were then coated with a thin layer of gold and imaged using a scanning electron microscope equipped with an energy dispersive X-ray analyzer (FEG-SEM Leo Supra 35, Oberkochen, Germany).

Preparation of the MWNT coated microarray substrate samples will be mentioned in section **3.5**. For SEM imaging, the MWNT coated microarray substrate samples were coated with a thin layer of platinum and imaged using a JEOL JSM 7000F field emission scanning electron microscope equipped with an energy dispersive X-ray analyzer (JEOL, Tokyo, Japan), in Faculty of Chemical & Metallurgical Engineering, ITU.

3.4.2 Fourier Transform Infrared Spectrometry (FT- IR)

Fourier transform infrared (FT-IR) spectra of functionalized samples were obtained on FTIR Spectrometer Bruker Equinox 55.

3.4.3 Dynamic Light Scattering (DLS)

The hydrodynamic radii of the functionalized and protein immobilized MWNTs were determined by dynamic light scattering (DLS) measurements which were performed with a Zetasizer NanoZS (Malvern Instruments, Malvern, UK) using a He−Ne laser as a light source with $\lambda = 632$ nm.

3.4.4. Atomic Force Microscopy (AFM)

The topology of the MWNT coated microarray substrate samples and protein immobilization on them was further analyzed by atomic force microscopy on an ambient AFM by Nanomagnetic Instruments (Oxford, UK).

3.5 Coating Glass Slides with Functional Groups

Although commercial microarray slides are available, some other slides with different functional groups are also prepared. Firstly, the glass slides were etched at room temperature for overnight and rinsed with ddH_2O. Then the slides were incubated in silaning solution including Ethanol, Acetic Acid and the desired silane chemical at room temperature for 10 hours. The slides were then washed extensively with 99% EtOH and ddH_2O, and dried with nitrogen gun.

3.6 Preparation of MWNT Coated Microarray Substrates

Prepared *8X_MWNT_NHS* solution was diluted to 4X-1/32X final concentrations using ddH_2O. Slides were placed in micro plate microarray apparatus

and 90 µl of solution was delivered into wells. Coating was achieved after 24 hours incubation at room temperature on a shaker platform at 350 rpm. The slides were then washed extensively with ddH_2O to remove loosely bound MWNTs on the surface.

3.7 Microarray Experiments

3.7.1 Antibody-arrays

3.7.1.1 Antibody & Antigen Samples

Monoclonal antibody pairs and purified antigens for C- reactive protein, purchased from Fitzgerald Industries International (Concord, MA, USA). All of the antibody and antigen samples are stored at -20º C until used.

3.7.1.2 Buffers

10 X PBS and Tween 20 were purchased from Sigma (USA). PBS-T (1 X PBS, 0.5% Tween 20) and PBS (1 X) were used for all washing steps. *Protein Dilution Buffer* (2% BSA in BPS-T) was used for dilution steps. *Protein Printing* and *Protein Blocking Buffers* were purchased from TeleChem International (Sunnyvale, CA, USA).

3.7.1.3 Array Printing & Hybridization

All capture antibodies were diluted to desired final concentrations using *Protein Printing Buffer*. Capture antibodies were spotted at 70% relative humidity using SMP3 pins, acquired from Telechem International and Omnigrid Accent Microarrayer (GeneMachine, San Carlos, CA, USA). Only one pin was used to ensure mechanical printing precision with agitated sonication-washing-drying cycles. Each antibody sample was spotted in triplicates. Spot diameter was 120 µm and space between spots for all dimensions was 500 µm. Spotted slides were incubated in humidity chamber providing >70% relative humidity for one hour. Slides were stored unprocessed at 4◦C and blocked with *Protein Blocking Buffer* for one hour just before the experiment. After one hour blocking, the slides were washed with PBS-T for 5 minutes, 1 X PBS for 10 minutes and dried using the slide centrifuge.

Antigen samples were diluted to desired final concentration in *Protein Dilution Buffer*. Slides were placed in micro plate microarray apparatus and 70 µl of solution was delivered into wells. The incubation was done at room temperature for one hour on a rotating shaker at 350 rpm. After incubation, wells were rinsed five times with PBS-T

and 1 X PBS. Biotinylated detection antibody samples with 2µg/ml concentration were prepared in *Protein Dilution Buffer* and added to the wells. After 1-h incubation with detection antibodies, wells were washed as before. As a last step, slides were incubated for 30 minutes with Cy3 conjugated streptavidin at 2 µg/ml concentration in *Protein Dilution Buffer* to generate fluorescence signal from the sandwiched structure. After incubation, the slides were washed with PBS-T for 5 minutes, 1 X PBS for 10 minutes. They were then dried using slide centrifuge and stored in dark until scanning.

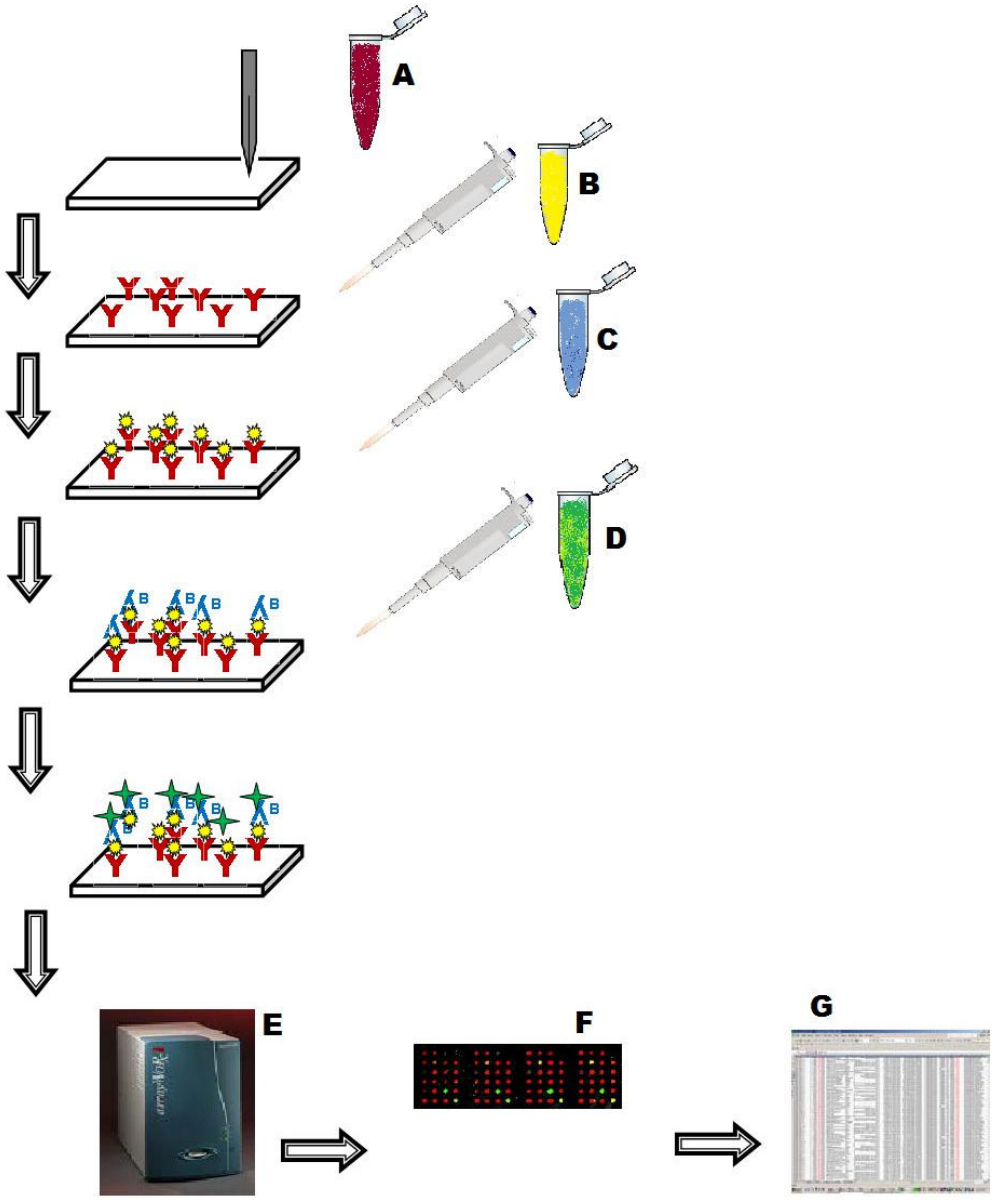

Fig 3.3. Antibody Microarray Experimental Scheme. **A-** Capture Ab printing on the slides. **B-**Antigen incubation. **C-** Biotinylated detection Ab incubation. **D-** Strep_Cy3 incubation. **E-** Scanning. **F-** Image Analysis. **G-** Data Analysis.

3.7.1.4 Image and Data Analysis

All slides were scanned under same exposure (0.2 s) in Cy3 channel with gain function "off" to obtain comparable images as manufacturer protocol suggested. About 5 μm resolution was selected for all slides. Scanner software was used for the analysis of the obtained images. All of the data anlaysis and graphing were done with the software OriginPro®8.

3.7.2 Oligo-arrays

3.7.2.1 Oligonucleotide Samples

QBP_38_F_1
Sequence (5'-3'): GGT CCA CCA CCA TGG TTG CCA TAC ATG CCA CCA TGG TC

QBP_38_F_2
Sequence (5'-3'): GAC CAT GGT GGC ATG TAT GGC AAC CAT GGT GGT GGA CC

QBP_38_R_1
Sequence (5'-3'): TCC AGA CCA TGG TGG CAT GTA TGG CAA CCA TGG TGG TG

QBP_38_R_2
Sequence (5'-3'): CAC CAC CAT GGT TGC CAT ACA TGC CAC CATGGT CTG GA

Firstly, 5′ phosphate groups of all oligonucleotide samples were amine-modified with an excess of ethylenediamine. **Fig 3.4** shows the amine modification steps.

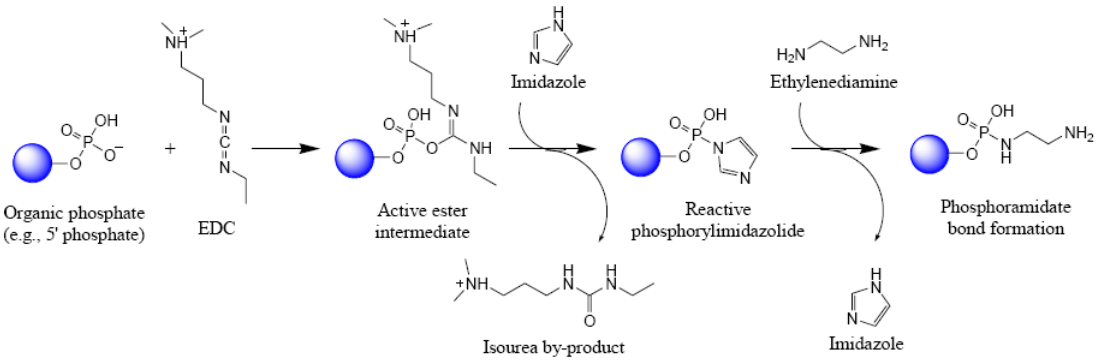

Fig 3.4. Amine-modification of Oligonucleotidea using Ethylenediamine, EDC, and Imidazole.

Then the oligonucleotides QBP_38_F_2 and QBP_38_R_2 which would be used as target samples are labeled with reactive fluorescent dyes of Cy5 and Cy3, respectively. All of the oligonucleotide samples are stored at -20º C until used.

3.7.2.2 Buffers

Stock Solutions

4X Oligo- Printing Buffer [600 mM sodium phosphate pH 8.5]

Dissolve the following in 90 ml of nuclease-free distilled water:

0.82 g Sodium phosphate monobasic (Sigma S0751)
7.57 g Sodium phosphate dibasic (Sigma S0876)

Adjust the pH to 8.5 using 1 N NaOH or 1 N HCl. Bring the final volume to 100 ml with nuclease-free distilled water.

Oligo- Blocking Solution [0.1 M Tris, 50 mM ethanolamine pH 9.0]

Dissolve the following in 90 ml of nuclease-free double distilled water:

6.055 g Trizma Base (Sigma T6791)
7.88 g Trizma HCl (Sigma T6666)
3.05 g (3.0 ml) Ethanolamine (Sigma E9508)

Adjust the pH to 9.0 using 6 N HCl. Bring final volume to 1 liter with double distilled water.

10% SDS

Dissolve 100 g Sodium dodecyl sulfate into 900 ml of nuclease-free distilled water. (Also called sodium lauryl sulfate, Sigma L4522) Heat slightly to solubilize the solid. Adjust the pH to 7.2 by adding a few drops of 5 N HCl. Bring the final volume to 1 liter.

20X SSC

Dissolve the following in 800 ml of nuclease-free distilled water:

175.3 g NaCl
88.2 g Sodium citrate

Adjust the pH to 7.0 5 N NaOH. Bring the final volume to 1 liter. Sterilize by autoclaving.

Post – Blocking Wash Solution

4X SSC, 0.1% SDS

Oligo- Hybridization Buffer

2 X SSC, 0.1% SDS

Post- Hybridization Wash Solutions

I. 2 X SSC, 0.1% SDS

II. 0.1 X SSC

III. 0 .01 X SSC

3.7.2.3 Array Printing & Hybridization

All capture oligonucleotide probes were diluted to 100- 6.25 µM final concentration using *Oligo- Printing Buffer*. Oligonucleotide probes were spotted at 70% relative humidity using SMP3 pins, acquired from Telechem International and Omnigrid Accent Microarrayer (GeneMachine, San Carlos, CA, USA). Only one pin was used to ensure mechanical printing precision with agitated sonication-washing-drying cycles. Each oligonucleotide probe was spotted in triplicates. Spot diameter was

120 µm and space between spots for all dimensions was 500 µm. Spotted slides were incubated in humidity chamber providing >70% relative humidity for overnight. Slides were stored unprocessed at 4◦C and blocked with pre- warmed *Oligo- Blocking Solution* for one hour just before the experiment. After one hour blocking, the slides were washed with pre- warmed *Post– Blocking Wash Solution* and dried using slide centrifuge.

Labeled oligonucleotide target samples were diluted to desired final concentration in *Oligo- Hybridization Buffer*. For the hybridization, LifterSlips are used. The LifterSlips are firstly cleaned with 100% EtoH and air dried. Then they are placed on the microarray slides, followed by pipetting the hybridization solution under the LifterSlips. The hybridization was carried out in a dark place at room temperature for 8 hours. An appropriate amount of blank hybridization buffer is added inside the hybridization chamber to insure > 70% humidity throughout the incubation. After hybridization, the slides were washed with *Post– Hybridization Wash Solutions I,II, and III,* respectively. The slides were then dried using slide centrifuge and stored in dark until scanning.

3.7.2.4 Image and Data Analysis

All slides were scanned with an ArrayWoRx(R) Biochip Reader (Applied Precision, Marlborough, UK) under same exposure (0.4 s) in Cy3 & Cy5 channels with gain function "off" to obtain comparable images as manufacturer protocol suggested. About 5 µm resolution was selected for all slides. Scanner software was used for the analysis of the obtained images. All of the data analysis and graphing were done with the software OriginPro®8.

4. RESULTS

4.1 Dispersion of MWNTs

A major barrier for developing and studying carbon nanotube based devices is the insolubility of CNTs in both aqueous and organic solvents and the resulting difficulty in processing them. Even the functionalized CNTs do not disperse in aqueous and organic solvents without assisting. The dispersion of CNTs can be assisted via two major approaches which are sonication and using surfactants as dispersing agents **[90, 91]**. MWNT_COOH was dispersed in ddH_2O by using the surfactant Triton X-100 and sonication. **Fig 4.1.A** shows the dispersion states reached via Triton X-100 and sonication. The best dispersion was reached with adding 0,1% Triton and 30 minutes sonication in a Bioblock Vibracell sonicator, so all of the dispersion steps were performed via this two step approach. **Fig 4.1.B** shows dispersed states of MWNT_NHS, MWNT_APTES, MWNT_COOH, and MWNT_OH. As seen the complete dispersion of MWNT_APTES in EtOH was not possible even via performed sonication and surfactant addition which is due to the high surface interaction between the APTES modified tubes **[92]**.

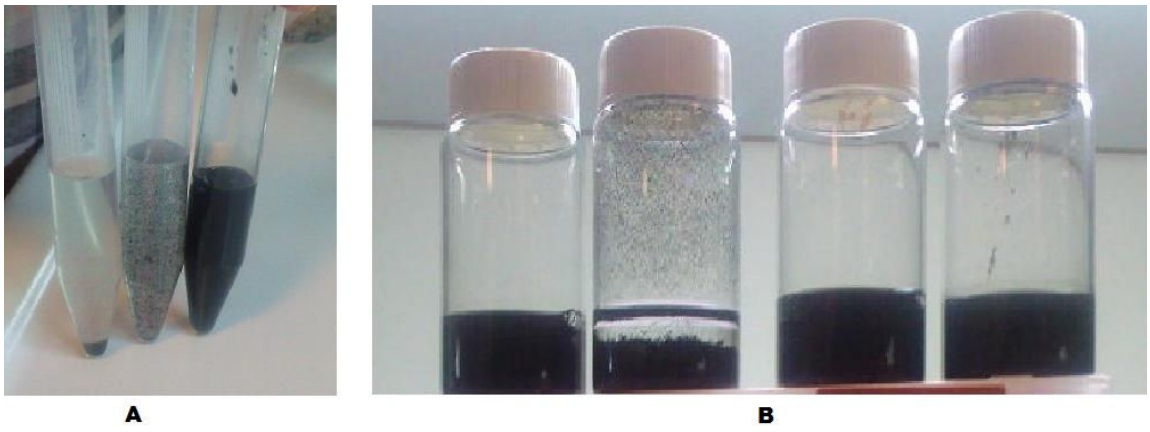

Fig 4.1. Dispersion of MWNTs. **(A)** MWNT_COOH in ddH_2O with no treatment (left), MWNT_COOH + Triton 100X (middle), MWNT_COOH + Triton 100X + Sonication (right). **(B)** MWNT_NHS in ddH_2O, MWNT_APTES in EtOH, MWNT_COOH in ddH_2O, MWNT_OH in ddH_2O, from left to right, respectively.

4.2 Characterization of Functionalized MWNTs

4.2.1 Dynamic Light Scattering

The size distribution of functionalized MWNTs was analyzed by dynamic light scattering experiments. Size distribution of the MWNTs is also a key for characterizing the efficiency of different functionalization steps and the achieved dispersion. **Fig 4.2** shows the size distribution of MWNT_COOH purchased from Arry Nanotechnology, with 20 nm diameter just as mentioned by the producer. The peak corresponding to ~4650 nm corresponds to the length of the MWNT_COOH.

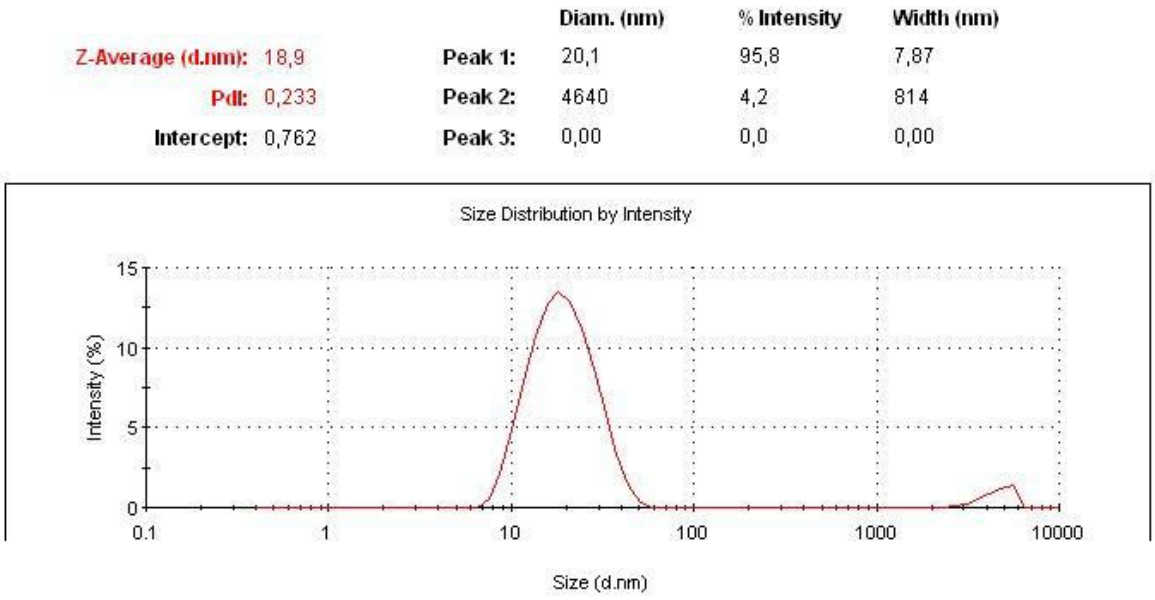

Fig 4.2. Size Distribution of MWNT_COOH purchased from Arry Nanotechnology.

Next steps of functionalization were also characterized via DLS. **Fig 4.3.** presents the EDC/ NHS treated oxidized *Baytubes*® **(A)** and the APTES modified MWNT_OH **(B)**. Both of the functionalization steps are not totally successful as resulting in functional group attachment to a limited percentage of ~ 26% of the MWNTs. On the other hand, treatment of MWNT_COOH with EDC/ NHS resulted in MWNT_NHS with ~ 65 nm diameter with an intensity of 100% **(Fig 4.4.)**. Therefore, MWNT_NHS functionalization was chosen for further protein immobilization and surface modification studies as the yield of this functionalization process was more than EDC/ NHS treatment of oxidized *Baytubes*® and the APTES modification of MWNT_OH.

			Diam. (nm)	% Intensity	Width (nm)
Z-Average (d.nm):	181	Peak 1:	19,2	74,2	2,49
PdI:	0,187	Peak 2:	64,1	25,8	6,96
Intercept:	0,831	Peak 3:	0,00	0,0	0,00

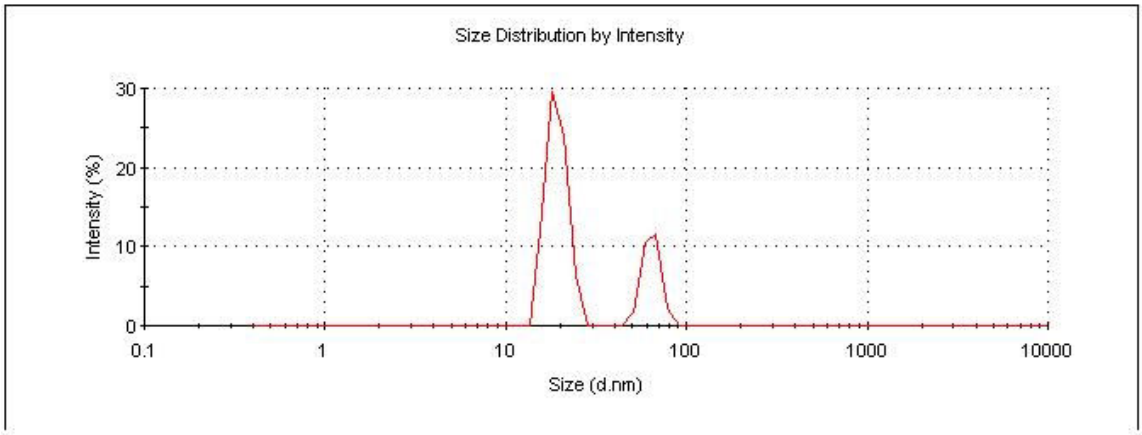

A

			Diam. (nm)	% Intensity	Width (nm)
Z-Average (d.nm):	39,2	Peak 1:	18,2	73,1	4,17
PdI:	0,083	Peak 2:	65,4	26,9	12,3
Intercept:	0,843	Peak 3:	0,00	0,0	0,00

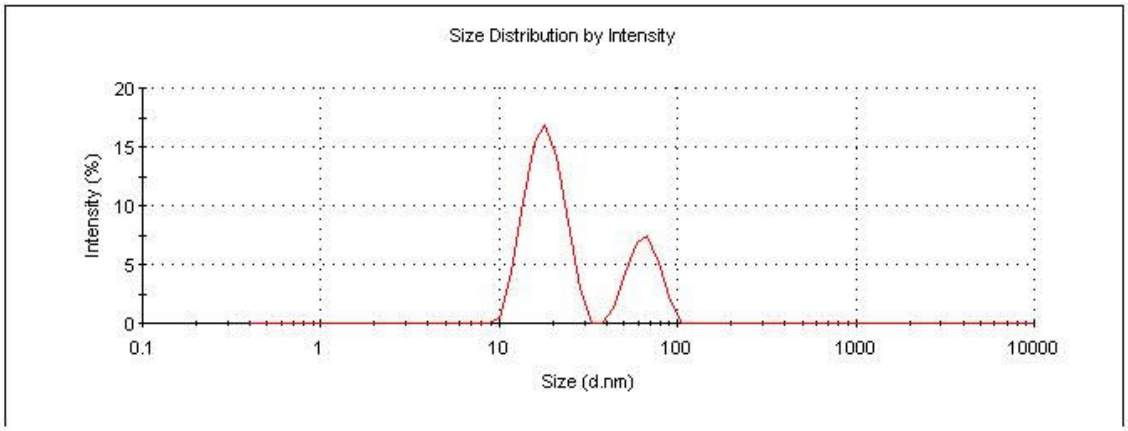

B

Fig 4.3. Size Distribution of oxidized *Baytubes*® after EDC/ NHS treatment **(A)**, and Size Distribution of APTES modified MWNT_OH **(B)**.

		Diam. (nm)	% Intensity	Width (nm)
Z-Average (d.nm): 61,5	Peak 1:	66,7	100,0	19,4
PdI: 0,104	Peak 2:	0,00	0,0	0,00
Intercept: 0,967	Peak 3:	0,00	0,0	0,00

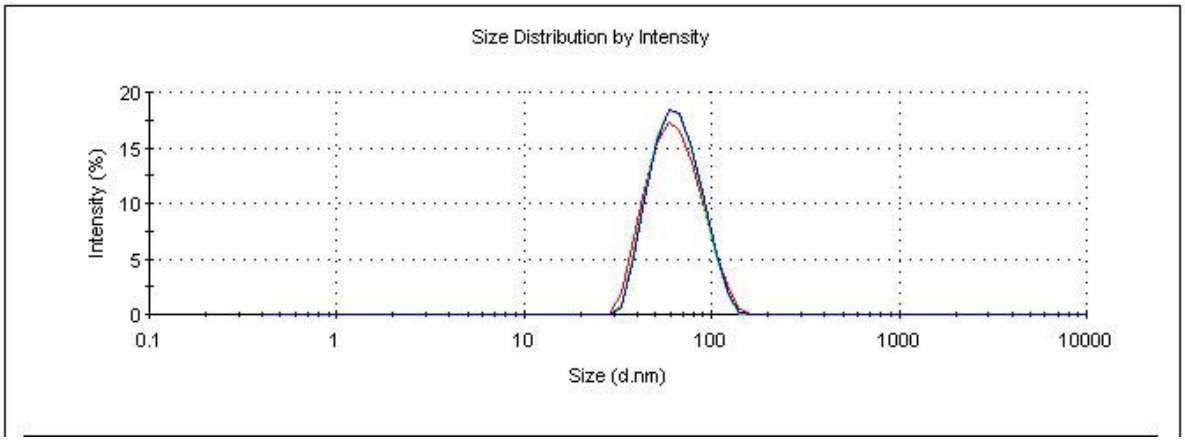

Fig 4.4. Size distribution of EDC/ NHS treated MWNT_COOH, (MWNT_NHS).

Protein immobilization on MWNT_NHS was performed using CRP Antibody as the model protein as mentioned in Materials & Experimental section. The process resulted in an MWNT_Protein conjugate with a diameter of ~365 nm with a 94% yield. Only 6% of the MWNT_NHS was not able to bind CRP_Cap_Ab.

		Diam. (nm)	% Intensity	Width (nm)
Z-Average (d.nm): 250	Peak 1:	367	93,9	195
PdI: 0,277	Peak 2:	60,1	6,1	15,1
Intercept: 0,743	Peak 3:	0,00	0,0	0,00

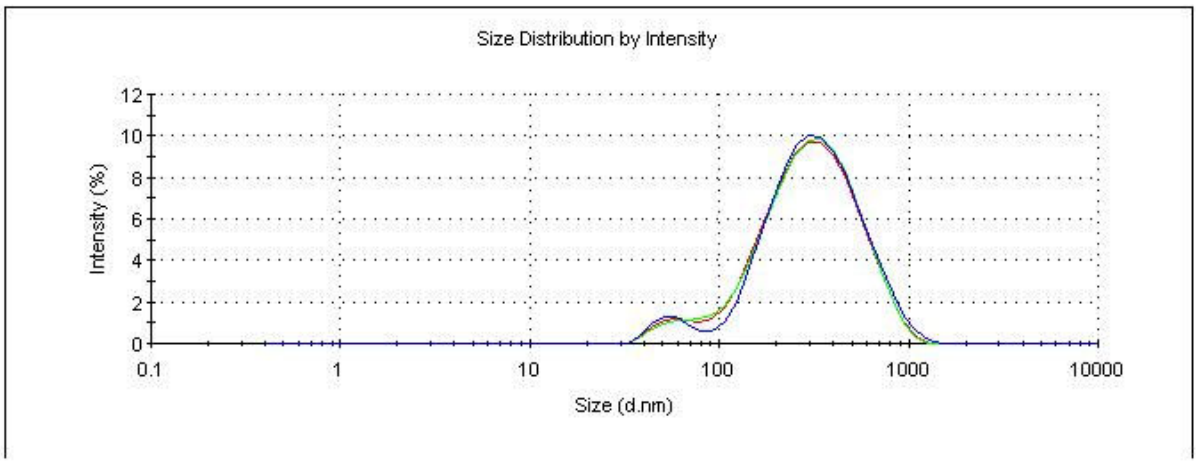

Fig 4.5. Size distribution of CRP_Cap_ Ab immobilized MWNT_NHS.

4.2.2 Fourier Transform Infrared Spectrometry

Each modification step is characterized using FT-IR to probe the vibrational changes during adsorption of proteins. **Fig 4.6.** shows the FT-IR spectrum of the MWNT-COOH, MWNT-OH, MWNT-NHS, and protein immobilized MWNTs. The assignments of the peaks are presented in **Table 4.1.** The protein immobilization on the MWNTs was evident from the appearance of the amide absorption peak at 1090 cm^{-1}.

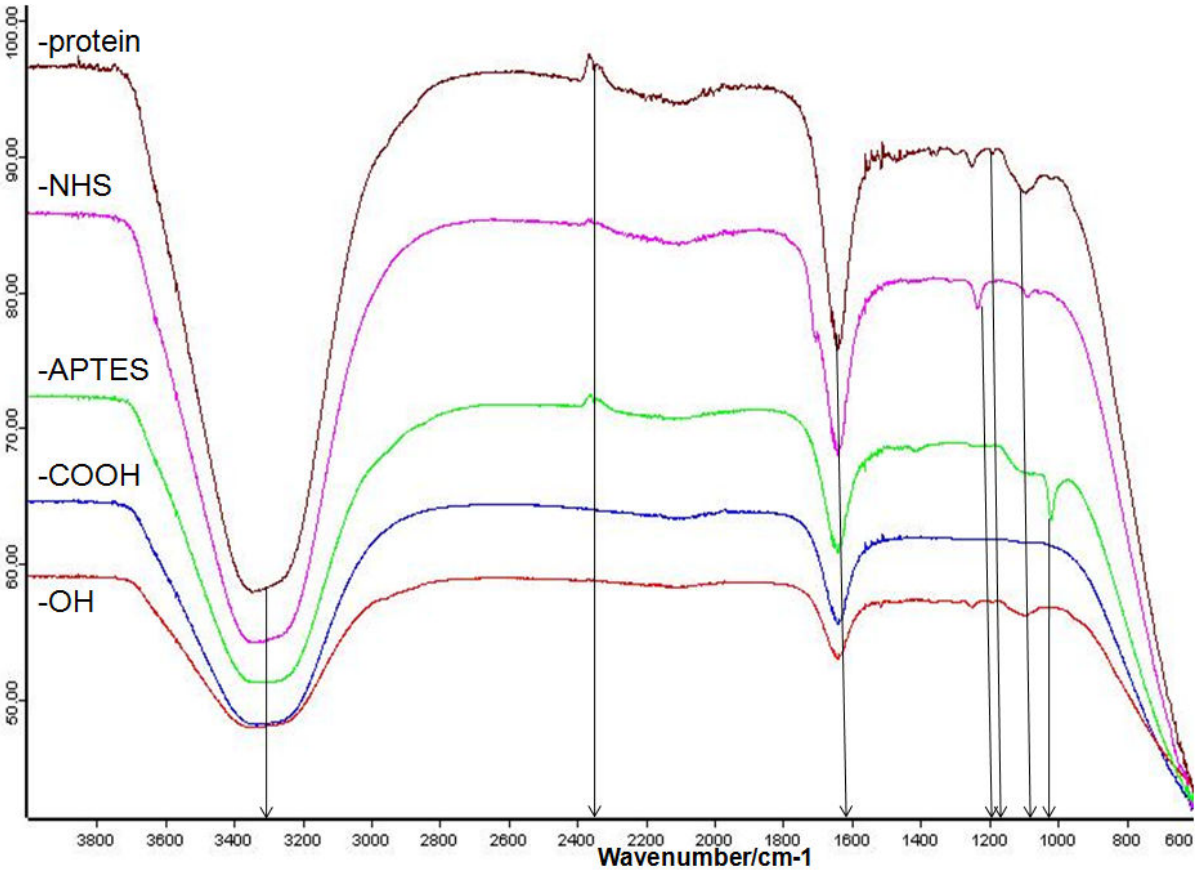

Fig 4.6. Transmission FTIR spectra of different functionalization steps.

Table 4.1. Assignment of the absorbencies in the FTIR spectra in **Fig 4.1.**

Assignment	Wavenumber/cm^{-1}	Reference
O-H Stretching	3300	**[93]**
H-bonded NH vibration band	2360	**[93]**
C= C Stretching	1625	**[94]**
Succinimide Group	1200	**[98]**
C-OH groups of serine, threonine, & tyrosine residues	1172	**[95]**
Protein Amide I Absorption	~1090	**[96]**
Si-OH Groups	1016	**[97]**

4.2.3 Scanning Electron Microscopy

SEM analyses were performed in order to further characterize the functionalized MWNTs. The predictable size of MWNT_NHS in the SEM image supports the DLS results. SEM image of MWNT_APTES shows non- homogenous functionalization of the nanotubes having different diameters, again supporting the DLS results indicating the low yield of the APTES functionalization **(Fig 4.7.)**.

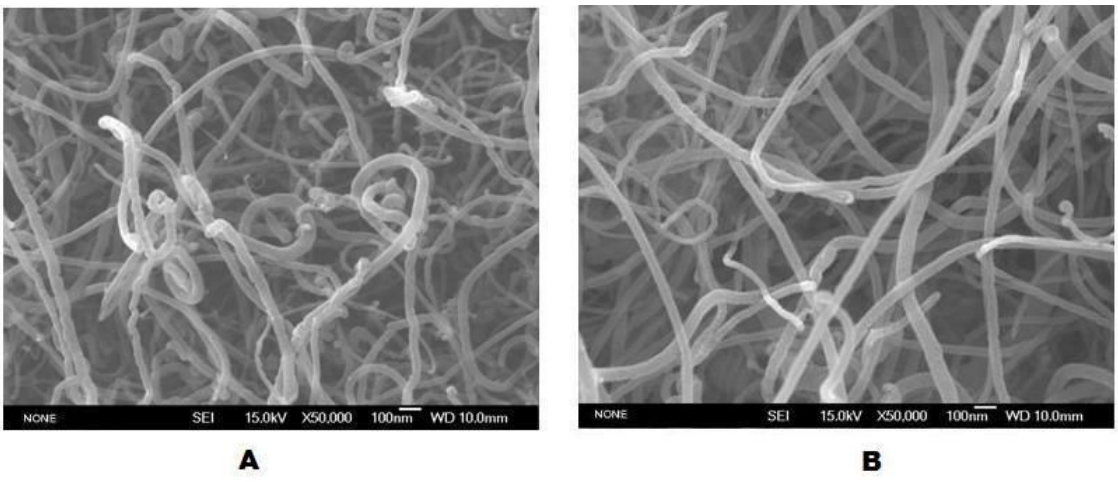

Fig 4.7. SEM images of MWNT_NHS **(A) and** MWNT_APTES **(B).**

Protein immobilization on MWNT_NHS is presented in **Fig 4.8.** It must be mentioned that imaging of MWNT_NHS at the same resolution as that of protein immobilized MWNTs was very difficult according to the change in conductivity on the surface of the MWNTs. Immobilized proteins on the surface of MWNTs are clearly seen in the image.

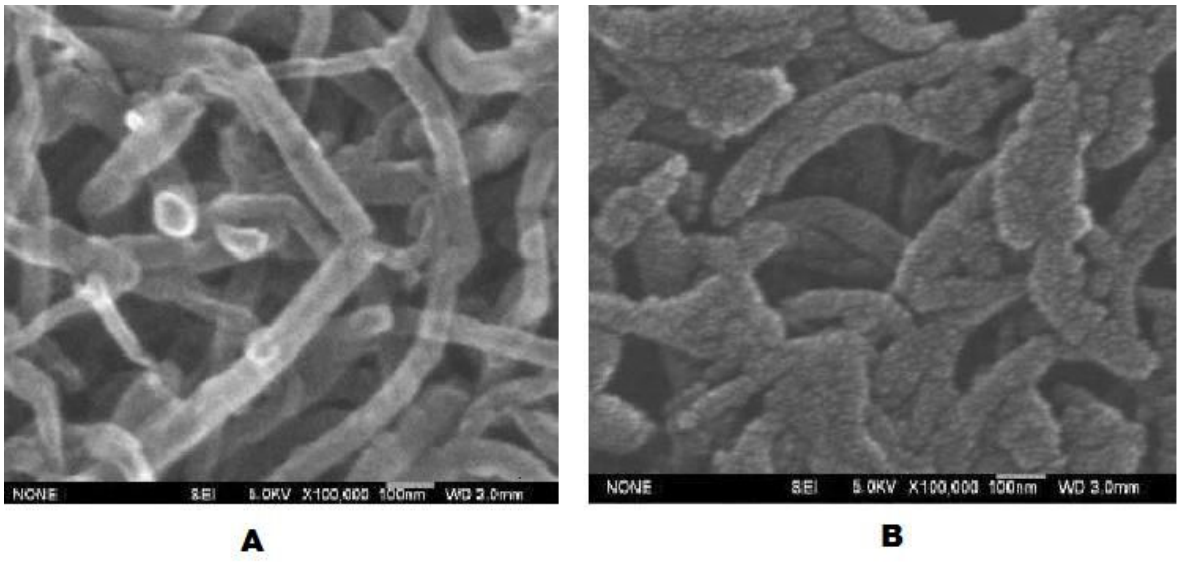

Fig 4.8. SEM images of MWNT- NHS before **(A)** and after protein immobilization **(B)**.

4.3 Microarray Experiments

4.3.1 Antibody Arrays

Coating of the microarray slides with different MWNT_NHS concentrations was performed as mentioned in **Section 3.6.** A sandwich type microarray experiment was performed in order to decide on the optimal MWNT_NHS concentration on the surface yielding the highest signal intensities. 8 different CRP_Cap_Ab concentrations were tried with each MWNT_NHS concentration on every slide. Among all the slides having different functional groups on their surface, the amine slide coated with *1/16X_MWNT_NHS* and the mercapto slide coated with *4X_MWNT_NHS* showed the highest intensities **(Fig 4.9.)**. Therefore, *1/16X_MWNT_NHS* coated amine slide and *4X_MWNT_NHS* coated mercapto slide were chosen for further experiments about the dynamic range of immobilized CRP_Cap_Ab on MWNT_NHS coated slide surfaces.

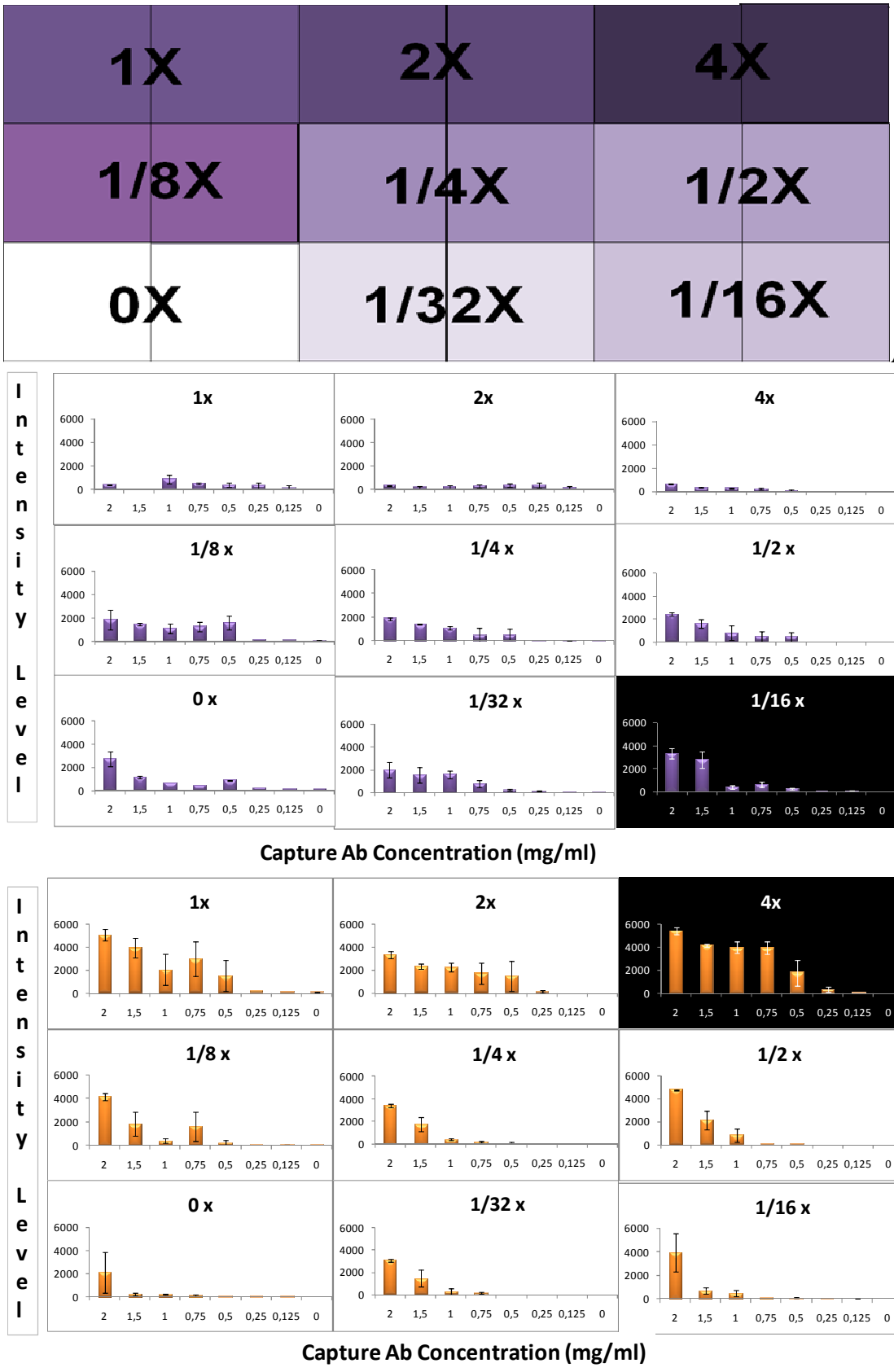

Fig 4.9. (A) Experimental Design for the coating of the slides with different MWNT_NHS concentrations. **(B)** Signal Intensities of the Amine Slide resulted from different MWNT_NHS coating concentrations. **(C)** Signal Intensities of the Mercapto Slide resulted from different MWNT_NHS coating concentrations.

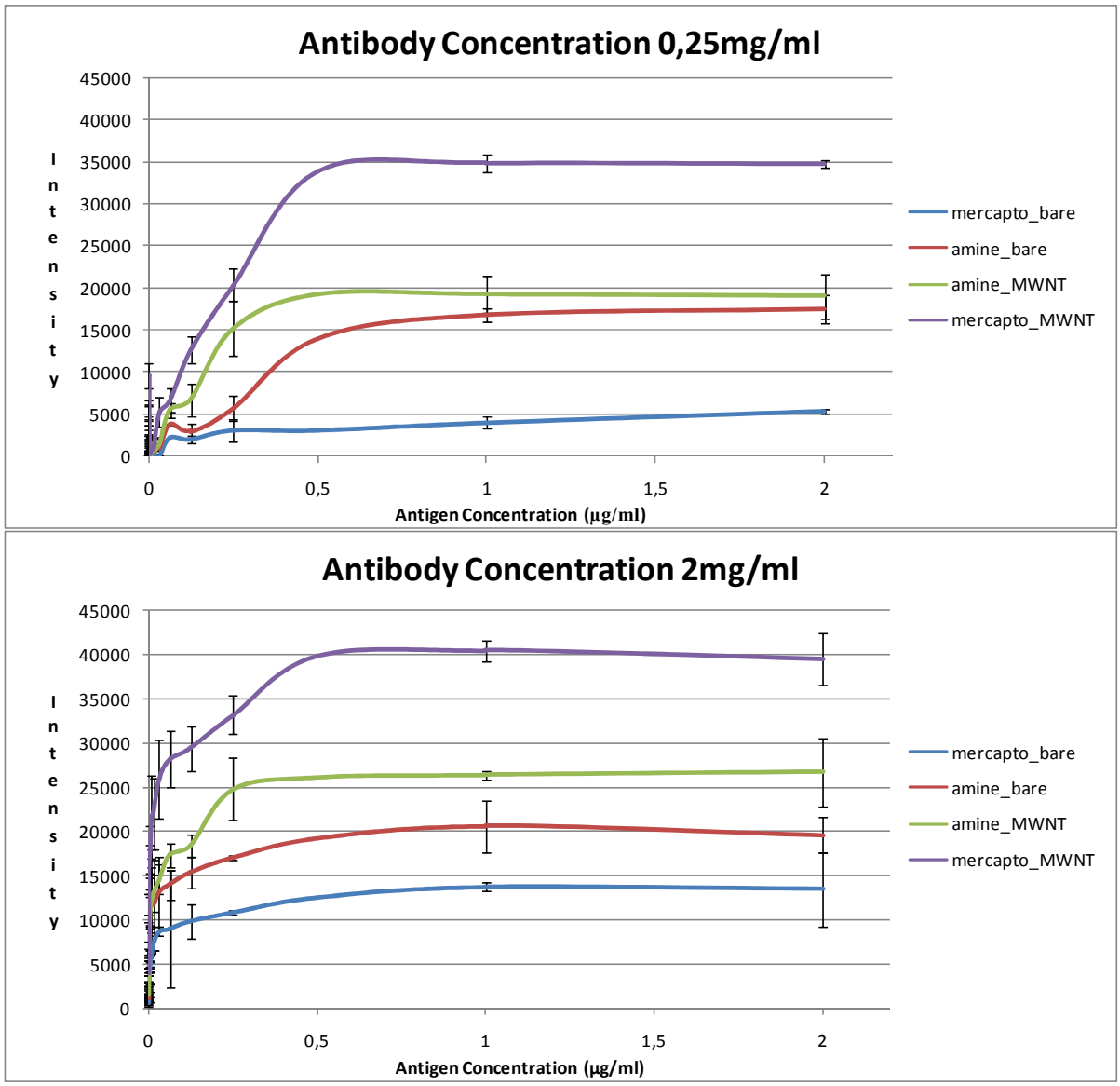

Fig 4.10. Comparative Standard Curves on bare and MWNT_NHS coated slides for 2mg/ml and 0,25 mg/ml CRP_Cap_Ab concentrations.

Experiments for standard curve generation were performed by using serial dilutions of CRP antigen to determine the dynamic range of each CRP_Cap_Ab concentration on MWNT coated and non-coated microarray slides as mentioned in **Section 3.7.1**. Standard curves, presented in **Fig 4.10** were calculated using spot intensity values after background subtraction. About 12 µm squares were selected from corners between spots on the slides for background calculations. Final spot intensities were calculated by subtracting reference spot intensity values from each antibody's spot

intensity. " Boltzmann Fit" parameter was used for the standard curve analysis **(Fig 4.11.)**. R^2 values for *1/16X_MWNT_NHS* coated amine slide were calculated as 0.9819, 0.9890, 0.9847, 0.9729, 0.9795, 0.9578, 0.9506 for CRP_Cap_Ab concentrations of 2, 1.5, 1, 0.75, 0.5, 0.25, 0.125mg/ml, respectively.

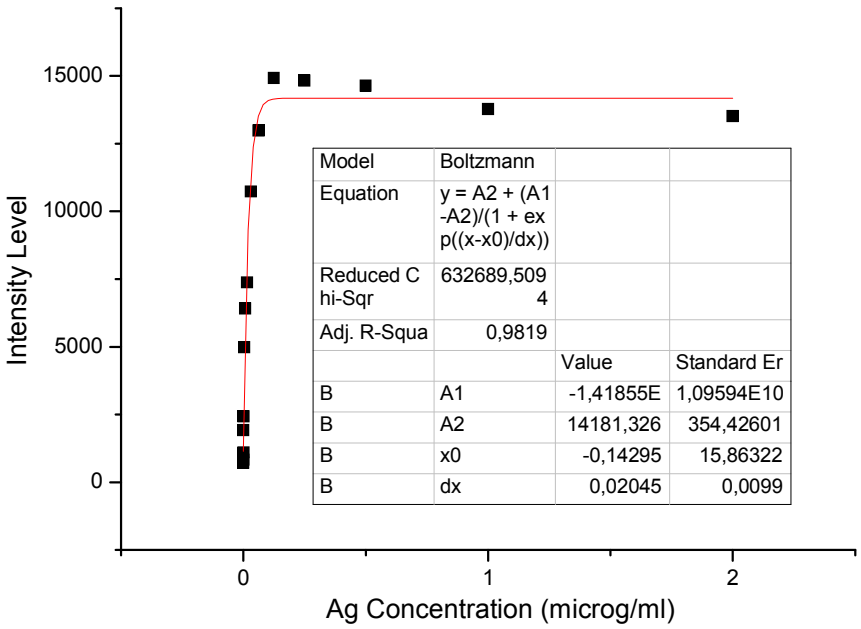

A

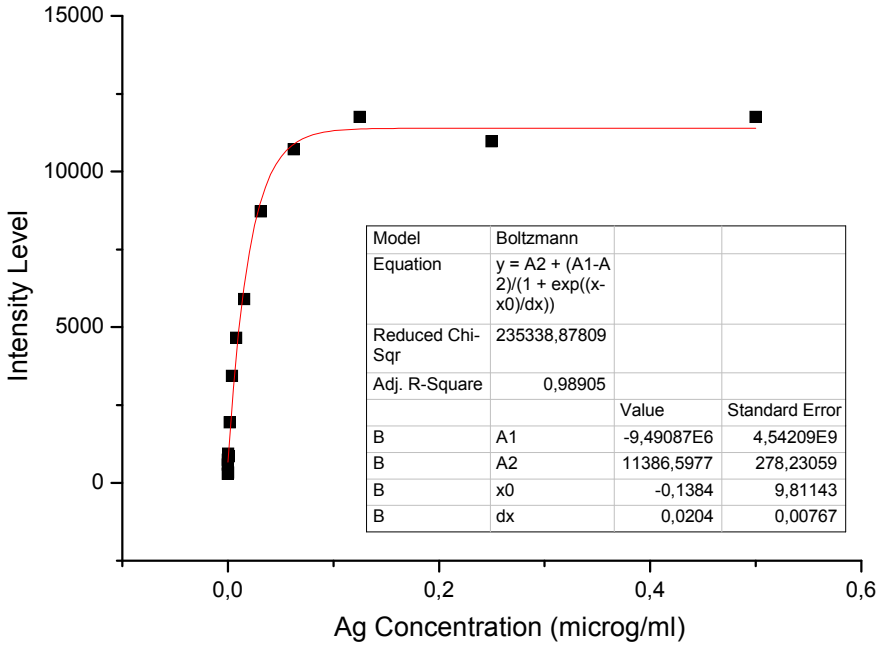

B

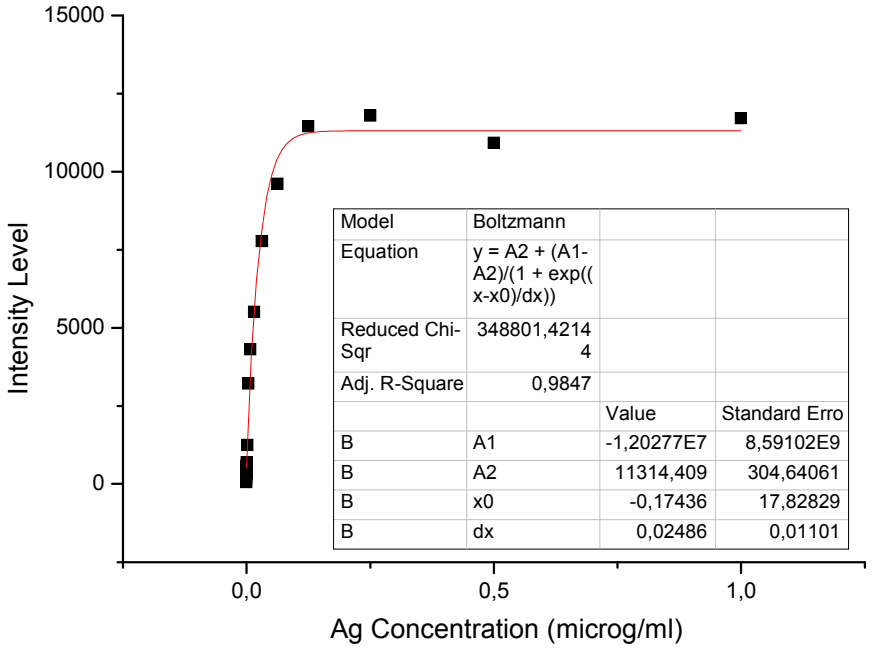
15000
10000
5000
0
Intensity Level
0,0
0,5
1,0
Ag Concentration (microg/ml)
Model Boltzmann
Equation y = A2 + (A1-A2)/(1 + exp((x-x0)/dx))
Reduced Chi-Sqr 348801,42144
Adj. R-Square 0,9847
Value Standard Erro
B A1 -1,20277E7 8,59102E9
B A2 11314,409 304,64061
B x0 -0,17436 17,82829
B dx 0,02486 0,01101

C

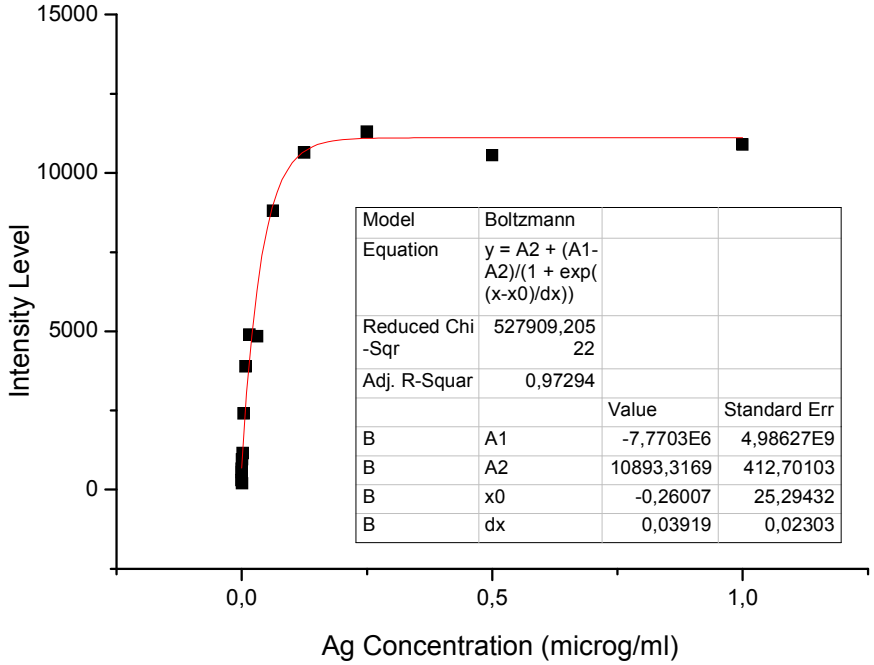
15000
10000
5000
0
Intensity Level
0,0
0,5
1,0
Ag Concentration (microg/ml)
Model Boltzmann
Equation y = A2 + (A1-A2)/(1 + exp((x-x0)/dx))
Reduced Chi-Sqr 527909,20522
Adj. R-Squar 0,97294
Value Standard Err
B A1 -7,7703E6 4,98627E9
B A2 10893,3169 412,70103
B x0 -0,26007 25,29432
B dx 0,03919 0,02303

D

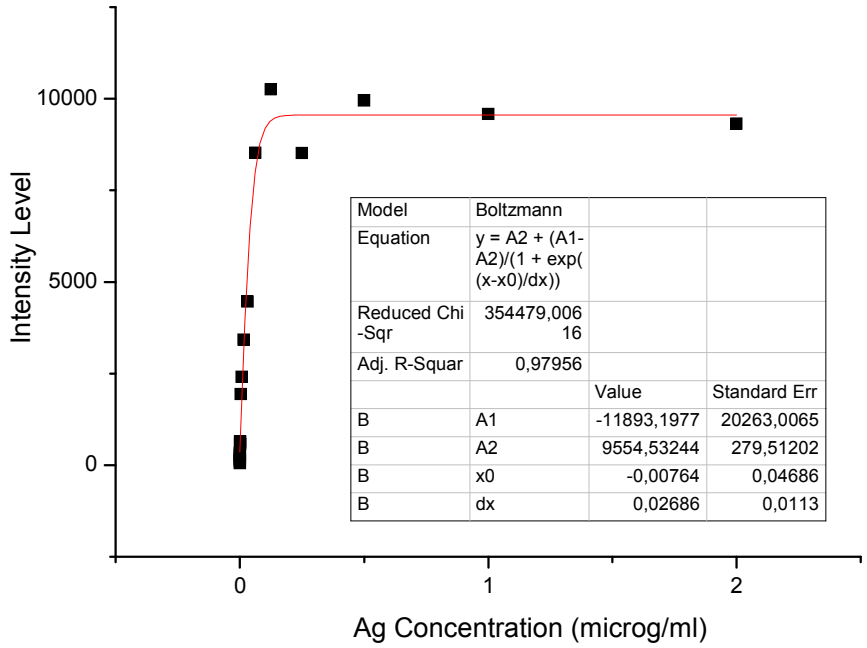
Intensity Level
10000
5000
0
0
1
2
Ag Concentration (microg/ml)
Model Boltzmann
Equation y = A2 + (A1-A2)/(1 + exp((x-x0)/dx))
Reduced Chi-Sqr 354479,00616
Adj. R-Squar 0,97956
Value Standard Err
B A1 -11893,1977 20263,0065
B A2 9554,53244 279,51202
B x0 -0,00764 0,04686
B dx 0,02686 0,0113

E

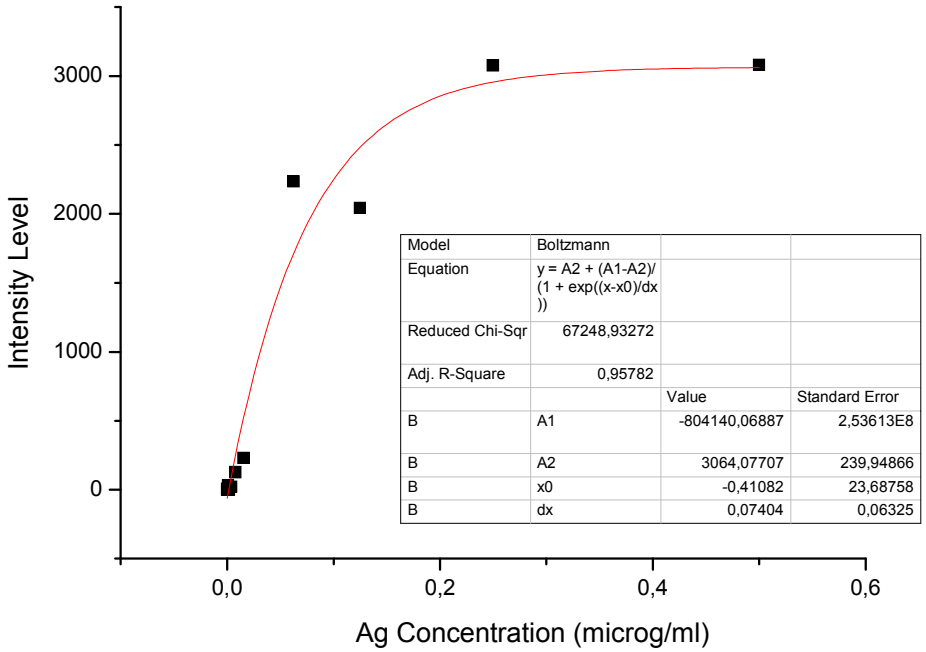
Intensity Level
3000
2000
1000
0
0,0
0,2
0,4
0,6
Ag Concentration (microg/ml)
Model Boltzmann
Equation y = A2 + (A1-A2)/(1 + exp((x-x0)/dx))
Reduced Chi-Sqr 67248,93272
Adj. R-Square 0,95782
Value Standard Error
B A1 -804140,06887 2,53613E8
B A2 3064,07707 239,94866
B x0 -0,41082 23,68758
B dx 0,07404 0,06325

F

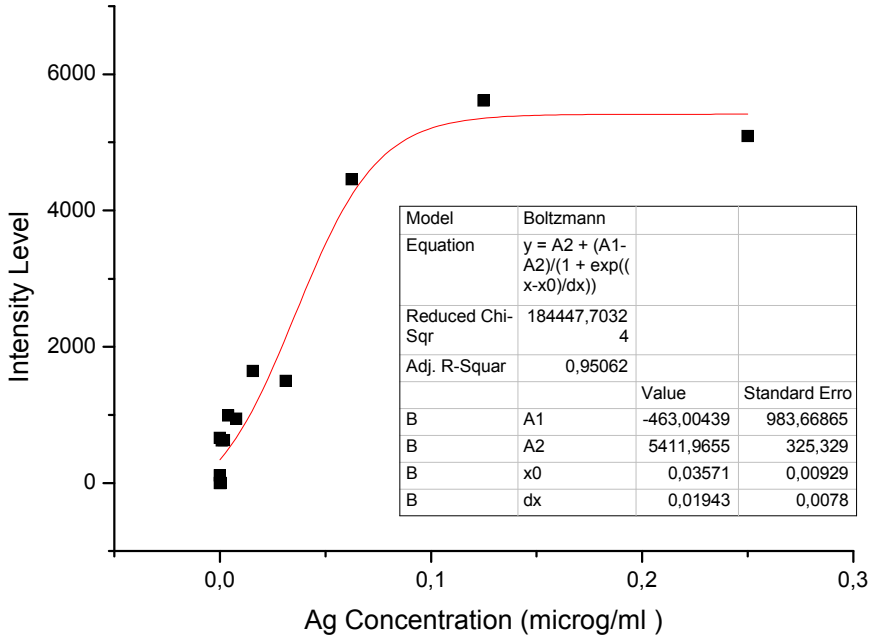

G

Fig 4.11. Boltzmann Regression Analysis of different CRP_Cap_Ab concentrations on *1/16X_MWNT_NHS* coated amine slide. **(A)** For CRP_Cap_Ab Concentration 2 mg/ml. **(B)** For CRP_Cap_Ab Concentration 1.5 mg/ml. **(C)** For CRP_Cap_Ab Concentration 1 mg/ml. **(D)** For CRP_Cap_Ab Concentration 0.75 mg/ml. **(E)** For CRP_Cap_Ab Concentration 0.5 mg/ml. **(F)** For CRP_Cap_Ab Concentration 0.25 mg/ml. **(G)** For CRP_Cap_Ab Concentration 0.125 mg/ml.

R^2 values for *4X_MWNT_NHS* coated mercapto slide were calculated as 0.9312, 0.9189, 0.9452, 0.9206, 0.9358, 0.9882, 0.9251 for CRP_Cap_Ab concentrations of 2, 1.5, 1, 0,75, 0,5, 0,25, 0,125mg/ml, respectively **(Fig 4.12.)**.

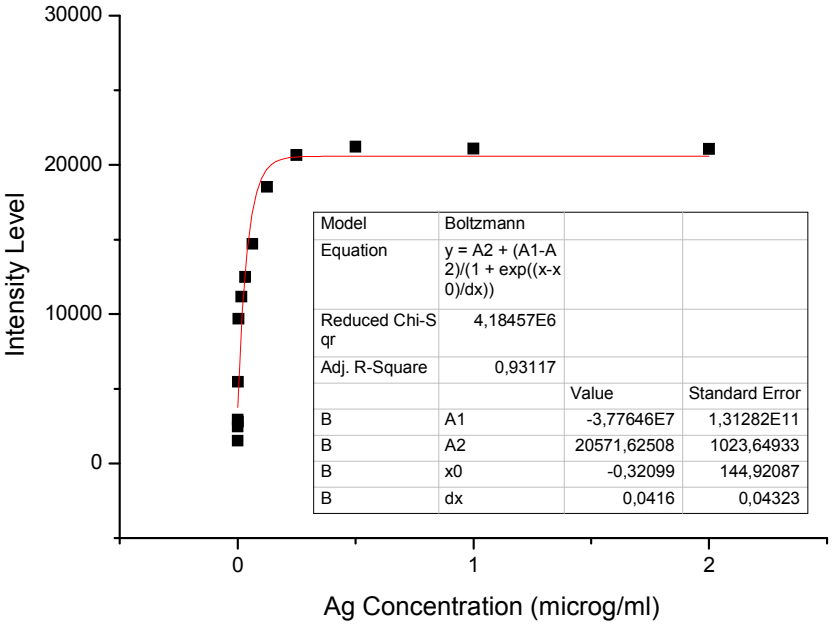

Model	Boltzmann		
Equation	y = A2 + (A1-A2)/(1 + exp((x-x0)/dx))		
Reduced Chi-Sqr	4,18457E6		
Adj. R-Square	0,93117		
		Value	Standard Error
B	A1	-3,77646E7	1,31282E11
B	A2	20571,62508	1023,64933
B	x0	-0,32099	144,92087
B	dx	0,0416	0,04323

A

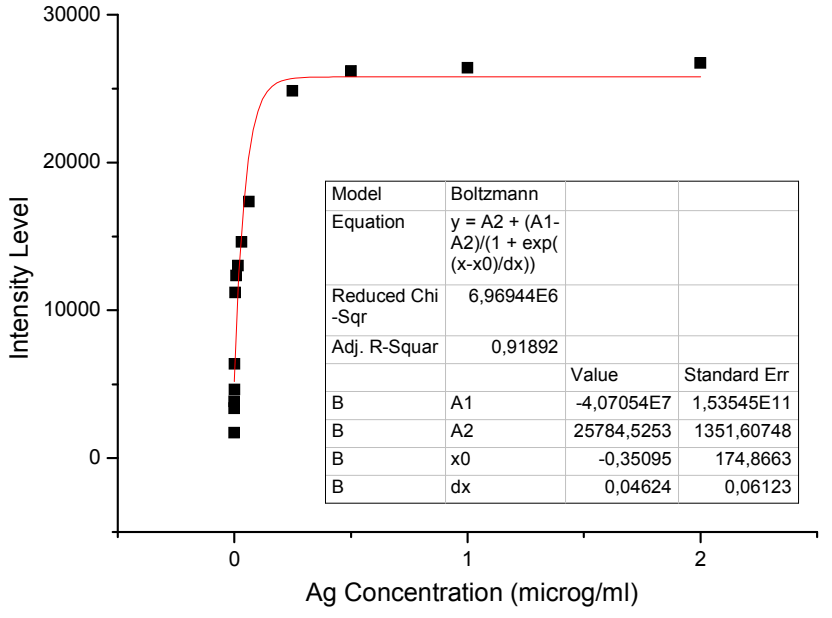

Model	Boltzmann		
Equation	y = A2 + (A1-A2)/(1 + exp((x-x0)/dx))		
Reduced Chi-Sqr	6,96944E6		
Adj. R-Squar	0,91892		
		Value	Standard Err
B	A1	-4,07054E7	1,53545E11
B	A2	25784,5253	1351,60748
B	x0	-0,35095	174,8663
B	dx	0,04624	0,06123

B

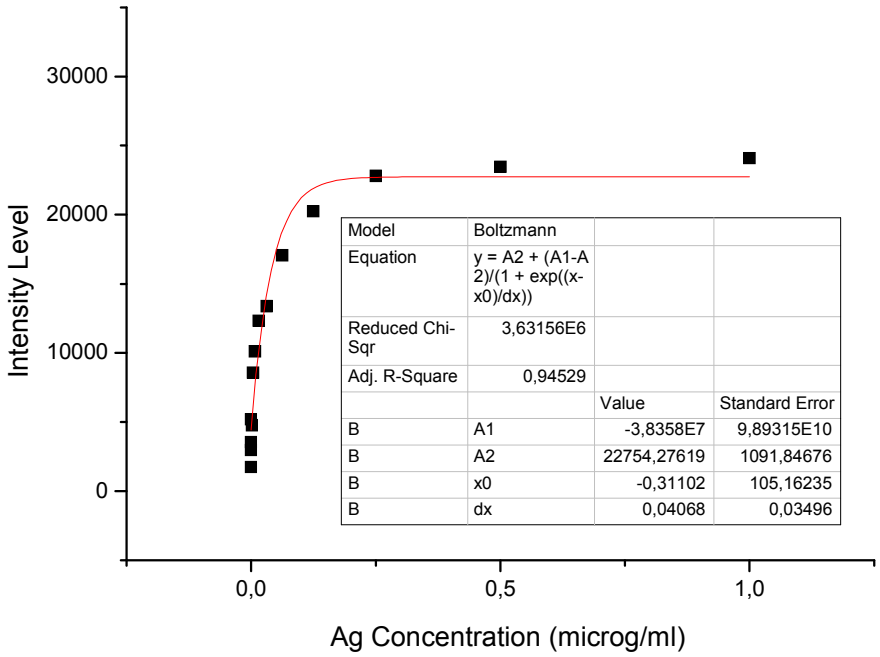
30000
20000
10000
0
Intensity Level
0,0
0,5
1,0
Ag Concentration (microg/ml)
Model Boltzmann
Equation y = A2 + (A1-A2)/(1 + exp((x-x0)/dx))
Reduced Chi-Sqr 3,63156E6
Adj. R-Square 0,94529
Value Standard Error
B A1 -3,8358E7 9,89315E10
B A2 22754,27619 1091,84676
B x0 -0,31102 105,16235
B dx 0,04068 0,03496

C

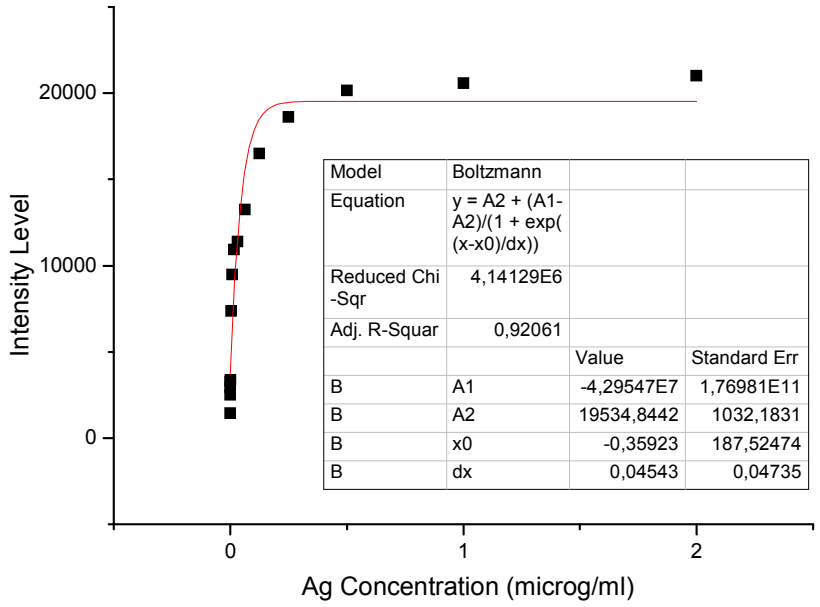
20000
10000
0
Intensity Level
0
1
2
Ag Concentration (microg/ml)
Model Boltzmann
Equation y = A2 + (A1-A2)/(1 + exp((x-x0)/dx))
Reduced Chi-Sqr 4,14129E6
Adj. R-Squar 0,92061
Value Standard Err
B A1 -4,29547E7 1,76981E11
B A2 19534,8442 1032,1831
B x0 -0,35923 187,52474
B dx 0,04543 0,04735

D

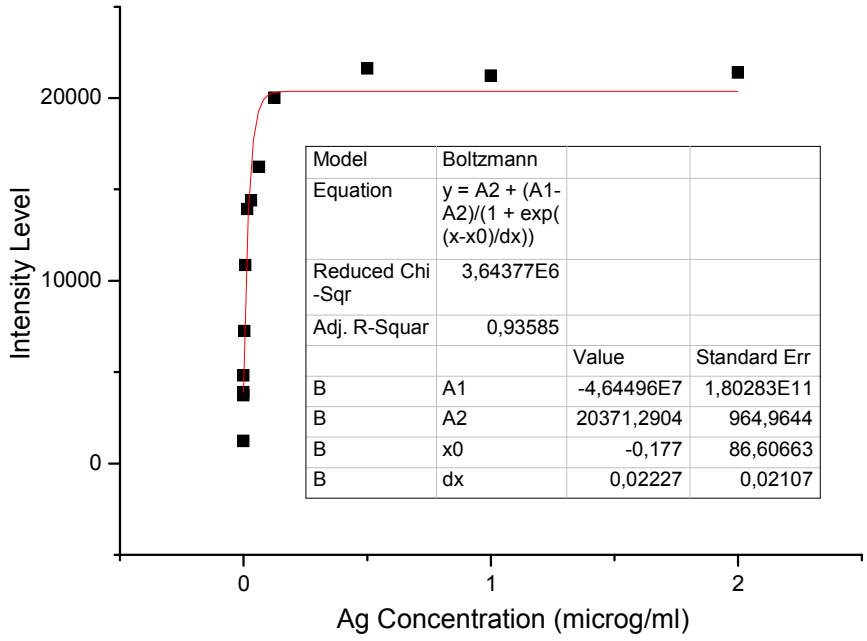
Intensity Level
20000
10000
0
0
1
2
Ag Concentration (microg/ml)
Model Boltzmann
Equation y = A2 + (A1-A2)/(1 + exp((x-x0)/dx))
Reduced Chi-Sqr 3,64377E6
Adj. R-Squar 0,93585
Value Standard Err
B A1 -4,64496E7 1,80283E11
B A2 20371,2904 964,9644
B x0 -0,177 86,60663
B dx 0,02227 0,02107

E

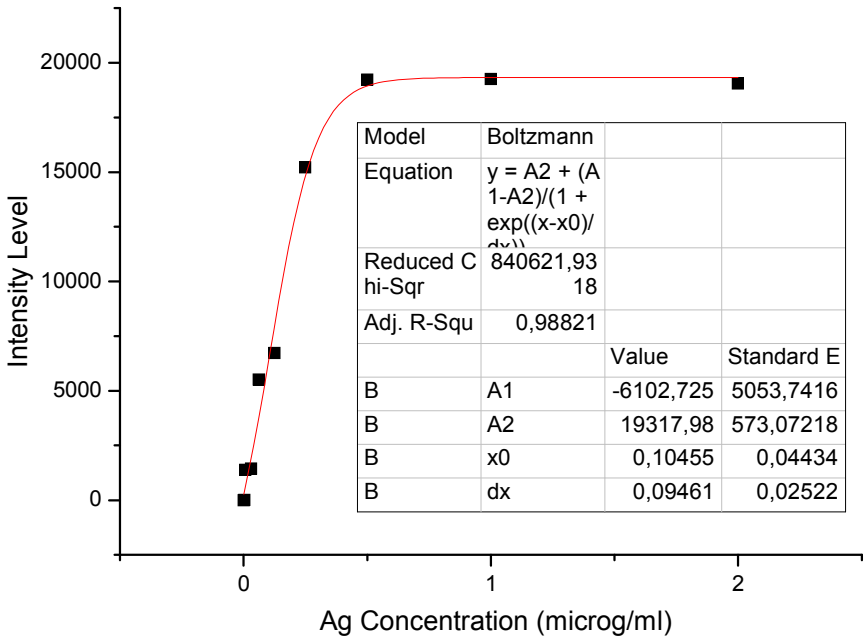
Intensity Level
20000
15000
10000
5000
0
0
1
2
Ag Concentration (microg/ml)
Model Boltzmann
Equation y = A2 + (A1-A2)/(1 + exp((x-x0)/dx))
Reduced Chi-Sqr 840621,9318
Adj. R-Squ 0,98821
Value Standard E
B A1 -6102,725 5053,7416
B A2 19317,98 573,07218
B x0 0,10455 0,04434
B dx 0,09461 0,02522

F

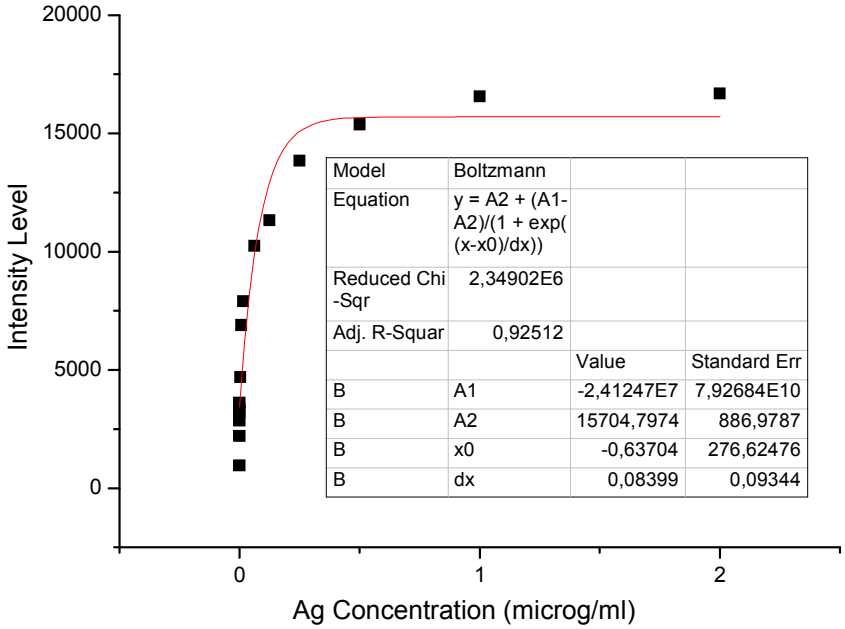

G

Fig 4.12. Boltzmann Regression Analysis of different CRP_Cap_Ab concentrations on *4X_MWNT_NHS* coated mercapto slide. **(A)** For CRP_Cap_Ab Concentration 2 mg/ml. **(B)** For CRP_Cap_Ab Concentration 1.5 mg/ml. **(C)** For CRP_Cap_Ab Concentration 1 mg/ml. **(D)** For CRP_Cap_Ab Concentration 0.75 mg/ml. **(E)** For CRP_Cap_Ab Concentration 0.5 mg/ml. **(F)** For CRP_Cap_Ab Concentration 0.25 mg/ml. **(G)** For CRP_Cap_Ab Concentration 0.125 mg/ml.

4.3.2 Oligonucleotide Arrays

As mercapto and amine slides yielded the highest intensities in antibody arrays, they were chosen for further oligonucleotide array experiments. Coating of the microarray slides with different MWNT_NHS concentrations was again performed as mentioned in **Section 3.6.** And similar to the antibody arrays, the first microarray experiments was performed in order to decide on the optimal MWNT_NHS concentration on the surface yielding the highest signal intensities. Eight different Probe Oligonucleotide concentrations were tried with each MWNT_NHS concentration on mercapto and amine slides. This experiment indicated that the amine slide coated with *1X_MWNT_NHS* and the mercapto slide coated with *4X_MWNT_NHS* revealing the highest intensities **(Fig 4.13.)**. Therefore, 1*X_MWNT_NHS* coated amine slide and

4X_MWNT_NHS coated mercapto slide were chosen for further experiments about the dynamic range of immobilized Probe Oligonucleotide Samples on MWNT_NHS coated slide surfaces.

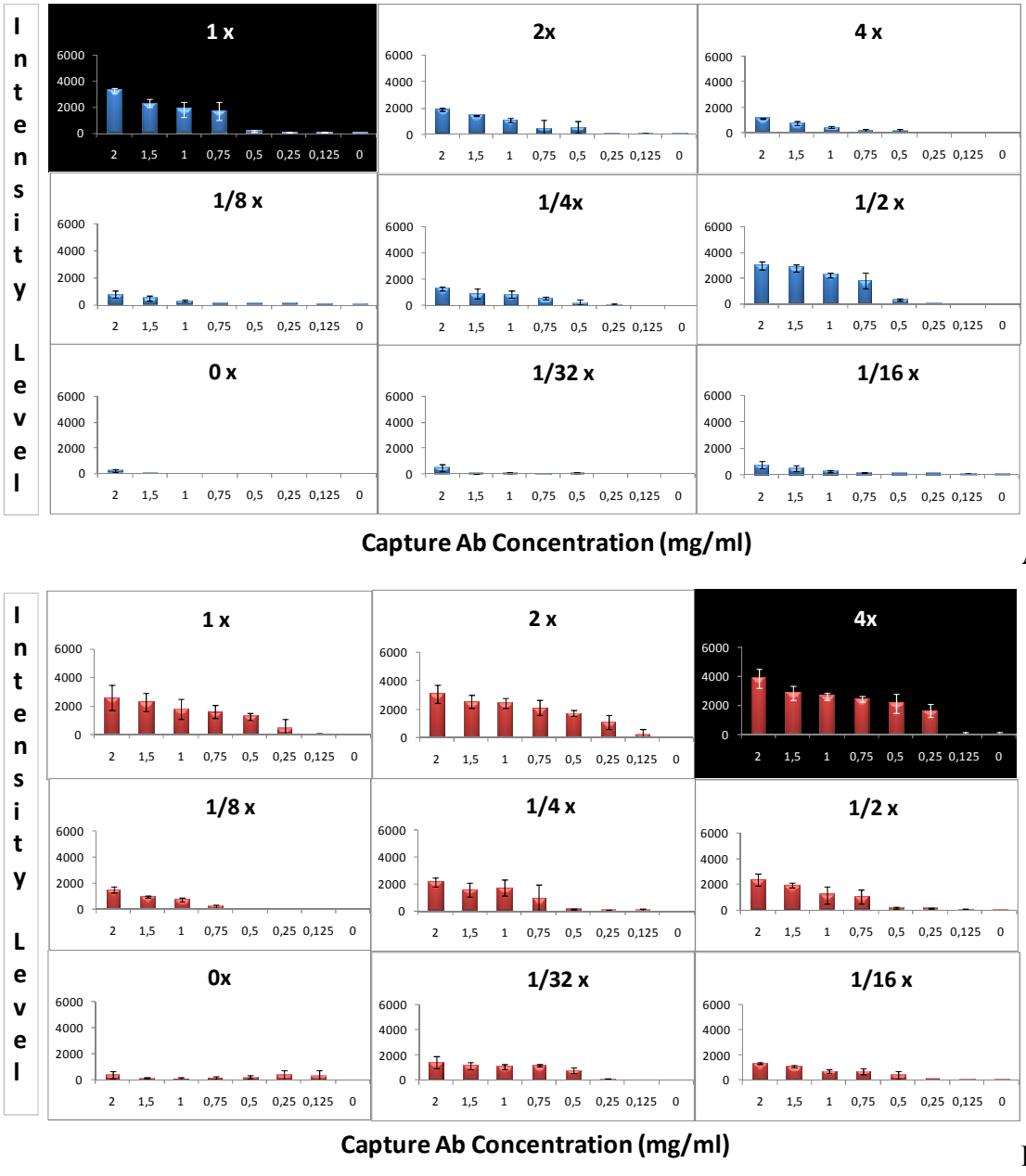

Fig 4.13. (A) Signal Intensities of the Amine Slide resulted from different MWNT_NHS coating concentrations. **(B)** Signal Intensities of the Mercapto Slide resulted from different MWNT_NHS coating concentrations.

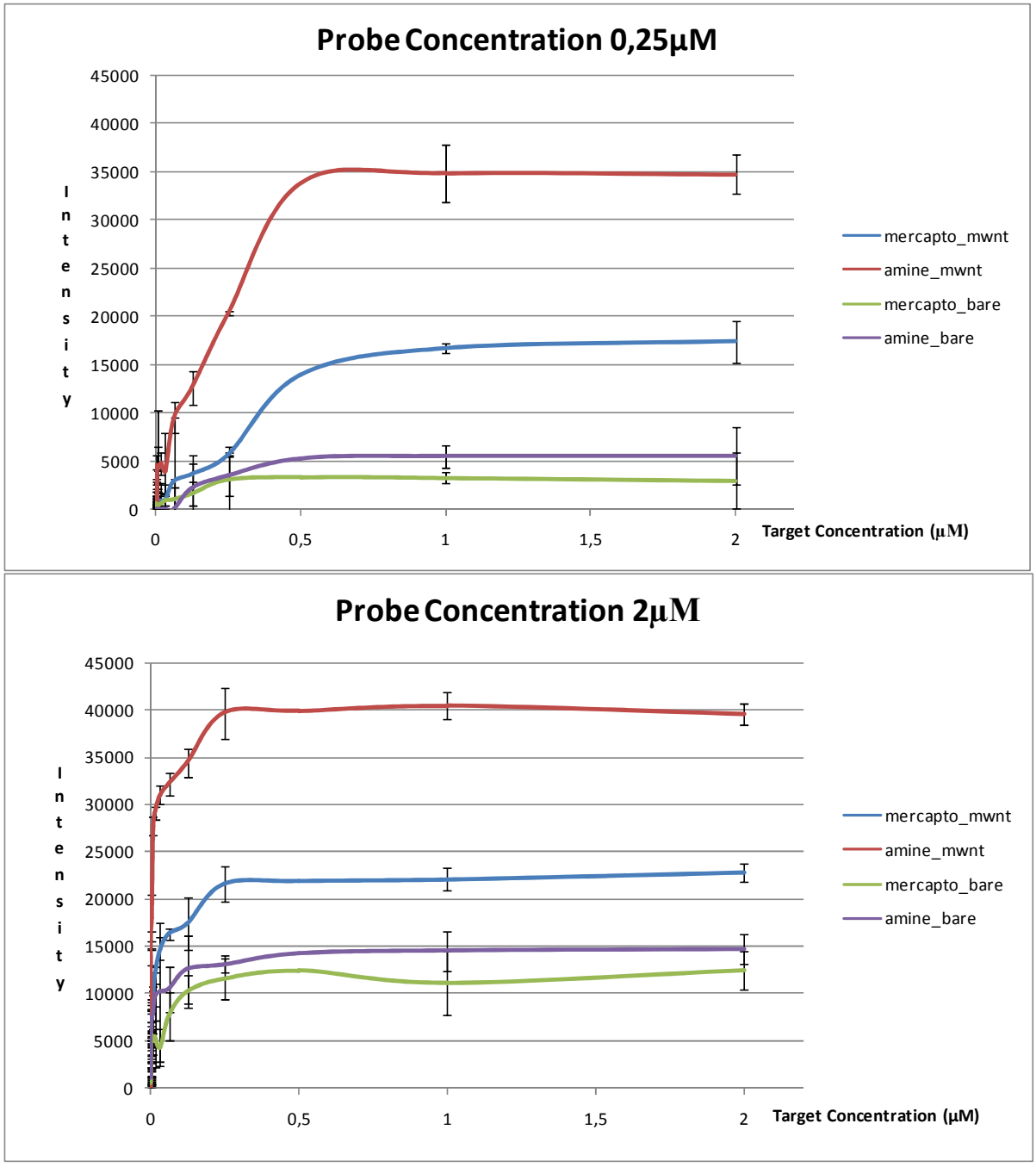

Fig 4.14. Comparative Standard Curves on bare and MWNT_NHS coated slides for 2µM and 0,25 µM Probe Oligonucleotide concentrations.

Experiments for standard curve generation were performed by using serial dilutions of Target Oligonucleotide samples to determine dynamic range of each probe Oligonucleotide concentration on MWNT coated and non-coated microarray slides as mentioned in **Section 3.7.2**. Standard curves, presented in **Fig 4.14.** were calculated just

like in antibody array analysis. “Boltzmann Fit” parameter was used for the standard curve analysis.

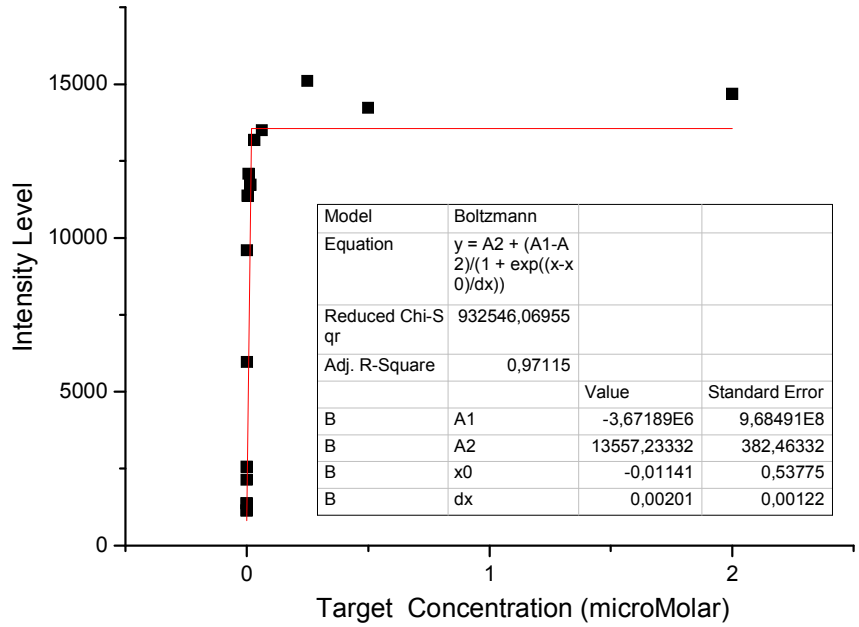

A

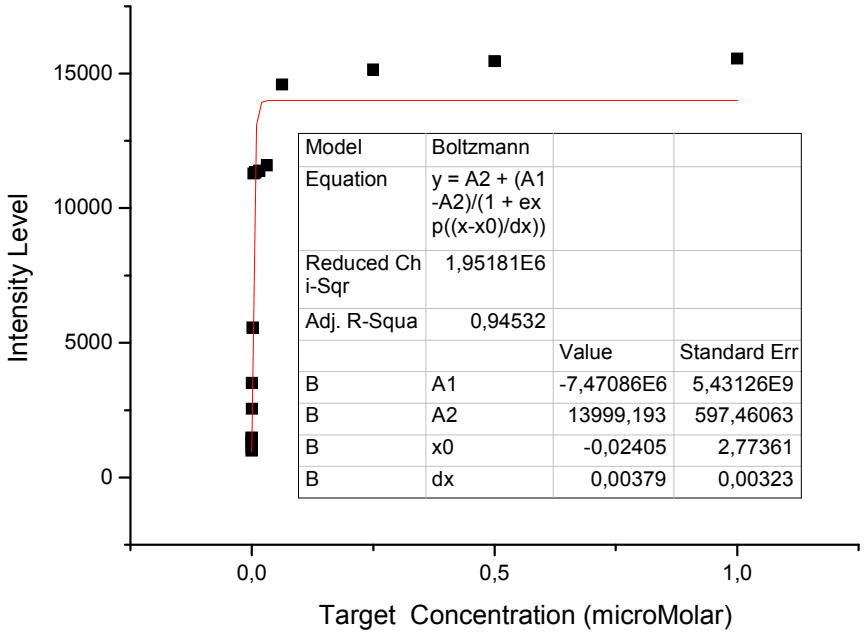

B

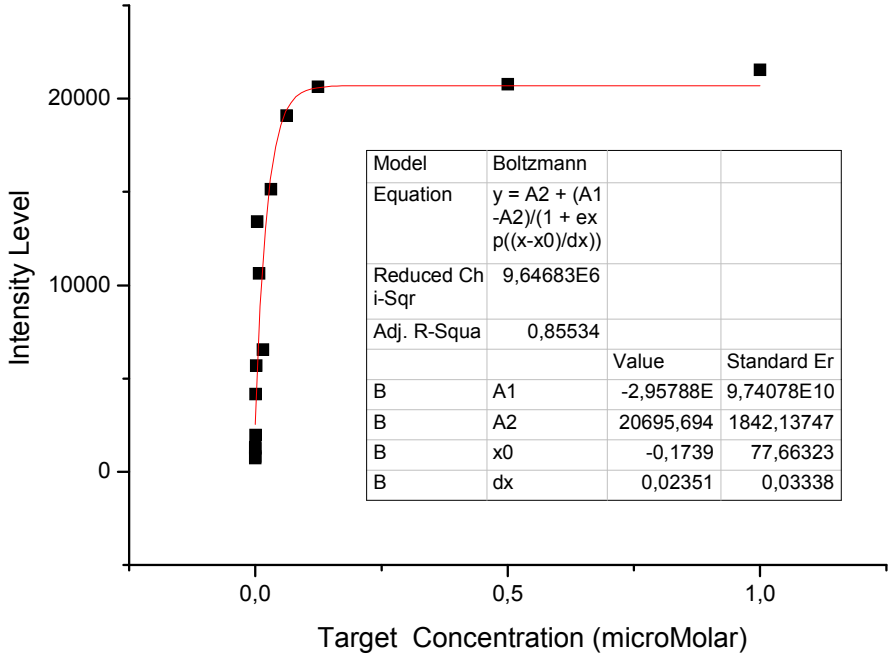
Intensity Level
20000
10000
0
0,0
0,5
1,0
Target Concentration (microMolar)
Model Boltzmann
Equation y = A2 + (A1 -A2)/(1 + exp((x-x0)/dx))
Reduced Chi-Sqr 9,64683E6
Adj. R-Squa 0,85534
Value Standard Er
B A1 -2,95788E 9,74078E10
B A2 20695,694 1842,13747
B x0 -0,1739 77,66323
B dx 0,02351 0,03338

C

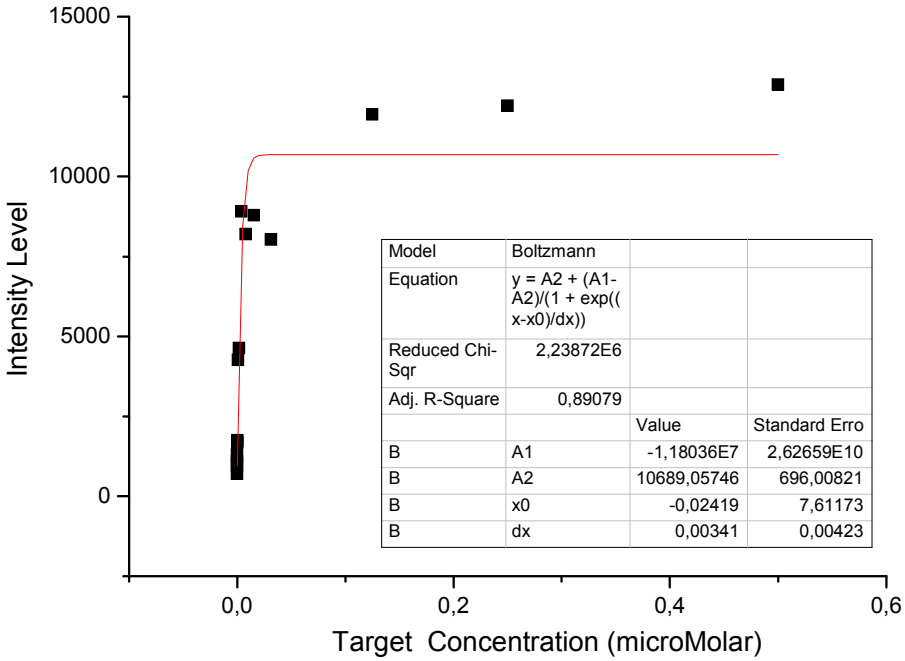
Intensity Level
15000
10000
5000
0
0,0
0,2
0,4
0,6
Target Concentration (microMolar)
Model Boltzmann
Equation y = A2 + (A1-A2)/(1 + exp((x-x0)/dx))
Reduced Chi-Sqr 2,23872E6
Adj. R-Square 0,89079
Value Standard Erro
B A1 -1,18036E7 2,62659E10
B A2 10689,05746 696,00821
B x0 -0,02419 7,61173
B dx 0,00341 0,00423

D

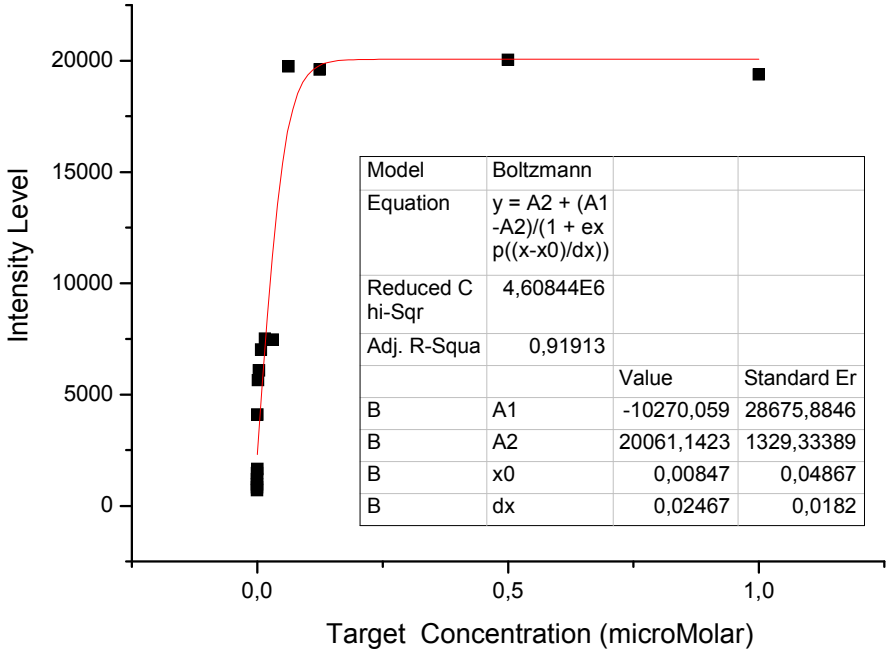
Intensity Level
20000
15000
10000
5000
0
0,0
0,5
1,0
Target Concentration (microMolar)
Model Boltzmann
Equation y = A2 + (A1 -A2)/(1 + exp((x-x0)/dx))
Reduced Chi-Sqr 4,60844E6
Adj. R-Squa 0,91913
Value Standard Er
B A1 -10270,059 28675,8846
B A2 20061,1423 1329,33389
B x0 0,00847 0,04867
B dx 0,02467 0,0182

E

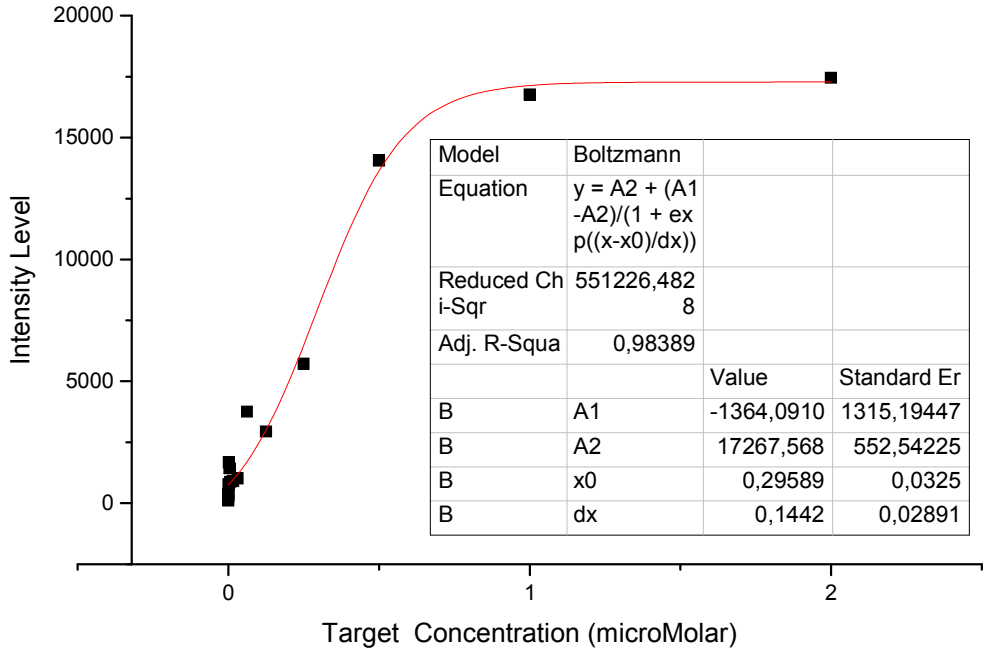
Intensity Level
20000
15000
10000
5000
0
0
1
2
Target Concentration (microMolar)
Model Boltzmann
Equation y = A2 + (A1 -A2)/(1 + exp((x-x0)/dx))
Reduced Chi-Sqr 551226,4828
Adj. R-Squa 0,98389
Value Standard Er
B A1 -1364,0910 1315,19447
B A2 17267,568 552,54225
B x0 0,29589 0,0325
B dx 0,1442 0,02891

F

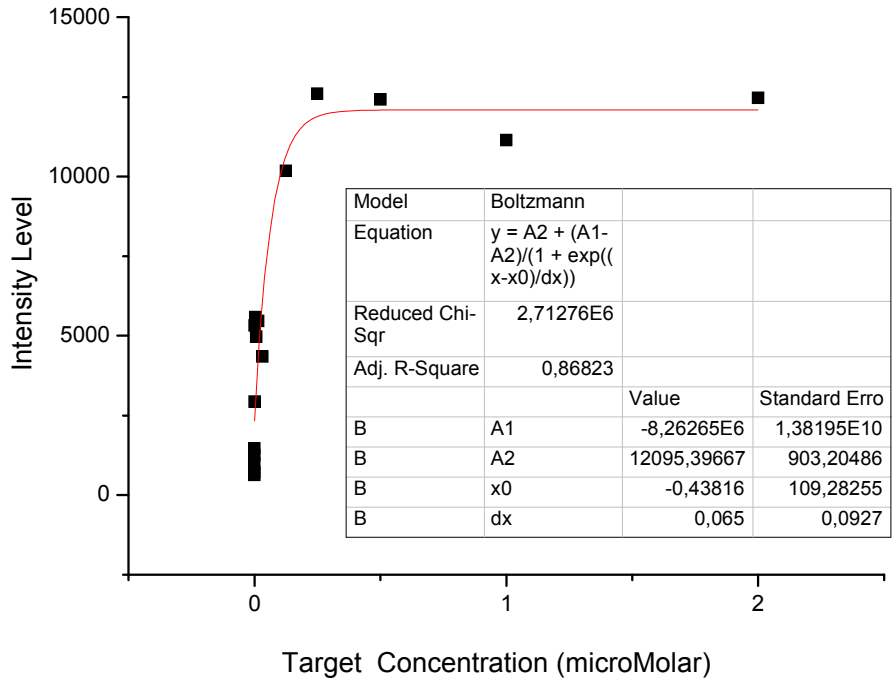

G

Fig 4.15. Boltzmann Regression Analysis of different Probe Oligonucleotide concentrations on *1X_MWNT_NHS* coated amine slide. **(A)** For Probe Oligonucleotide Concentration 2 mg/ml. **(B)** For Probe Oligonucleotide Concentration 1.5 mg/ml. **(C)** For Probe Oligonucleotide Concentration 1 mg/ml. **(D)** For Probe Oligonucleotide Concentration 0.75 mg/ml. **(E)** For Probe Oligonucleotide Concentration 0.5 mg/ml. **(F)** For Probe Oligonucleotide Concentration 0.25 mg/ml. **(G)** For Probe Oligonucleotide Concentration 0.125 mg/ml.

R^2 values for *1X_MWNT_NHS* coated amine slide were calculated as 0.9711, 0.9453, 0.8553, 0.8908, 0.9192, 0.9839, 0.8682 for Probe Oligonucleotide concentrations of 2, 1.5, 1, 0.75, 0.5, 0.25, 0.125 µM, respectively **(Fig 4.15.)**.

R^2 values for *4X_MWNT_NHS* coated mercapto slide were calculated as 0.9615, 0.9735, 0.987, 0.9508, 0.9516, 0.9929, 0.8718 for Probe Oligonucleotide concentrations of 2, 1, 1.5, 0.75, 0.5, 0.25, 0.125 µM, respectively **(Fig 4.16.)**.

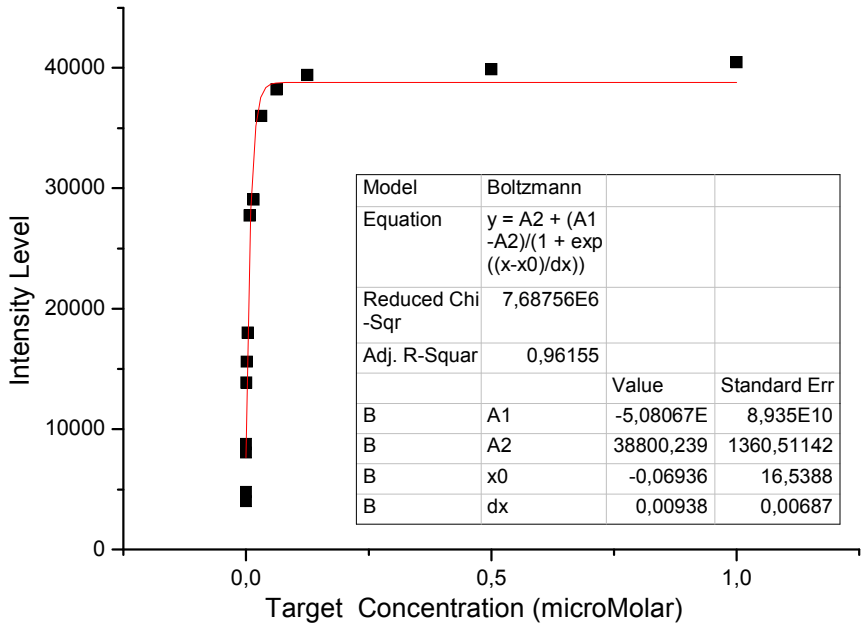
Intensity Level
40000
30000
20000
10000
0
0,0
0,5
1,0
Target Concentration (microMolar)
Model Boltzmann
Equation y = A2 + (A1 -A2)/(1 + exp ((x-x0)/dx))
Reduced Chi -Sqr 7,68756E6
Adj. R-Squar 0,96155
Value Standard Err
B A1 -5,08067E 8,935E10
B A2 38800,239 1360,51142
B x0 -0,06936 16,5388
B dx 0,00938 0,00687

A

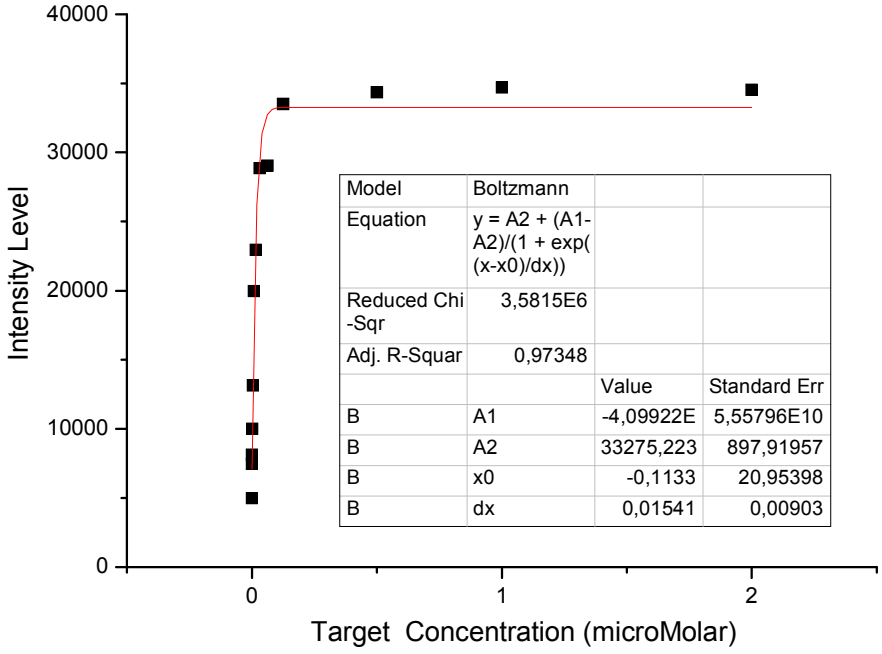
Intensity Level
40000
30000
20000
10000
0
0
1
2
Target Concentration (microMolar)
Model Boltzmann
Equation y = A2 + (A1-A2)/(1 + exp((x-x0)/dx))
Reduced Chi -Sqr 3,5815E6
Adj. R-Squar 0,97348
Value Standard Err
B A1 -4,09922E 5,55796E10
B A2 33275,223 897,91957
B x0 -0,1133 20,95398
B dx 0,01541 0,00903

B

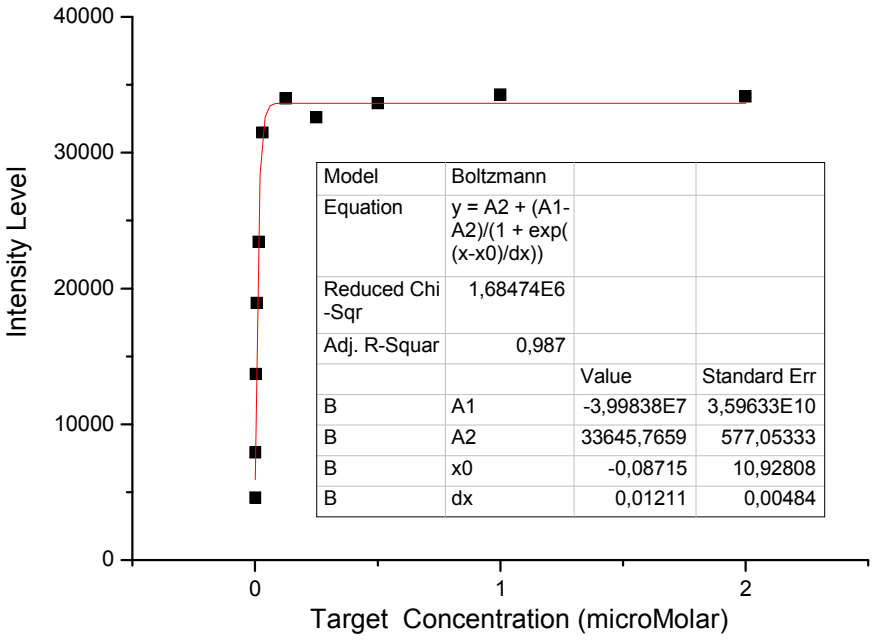
40000
30000
20000
10000
0
Intensity Level
0
1
2
Target Concentration (microMolar)
Model Boltzmann
Equation y = A2 + (A1-A2)/(1 + exp((x-x0)/dx))
Reduced Chi-Sqr 1,68474E6
Adj. R-Squar 0,987
Value Standard Err
B A1 -3,99838E7 3,59633E10
B A2 33645,7659 577,05333
B x0 -0,08715 10,92808
B dx 0,01211 0,00484

C

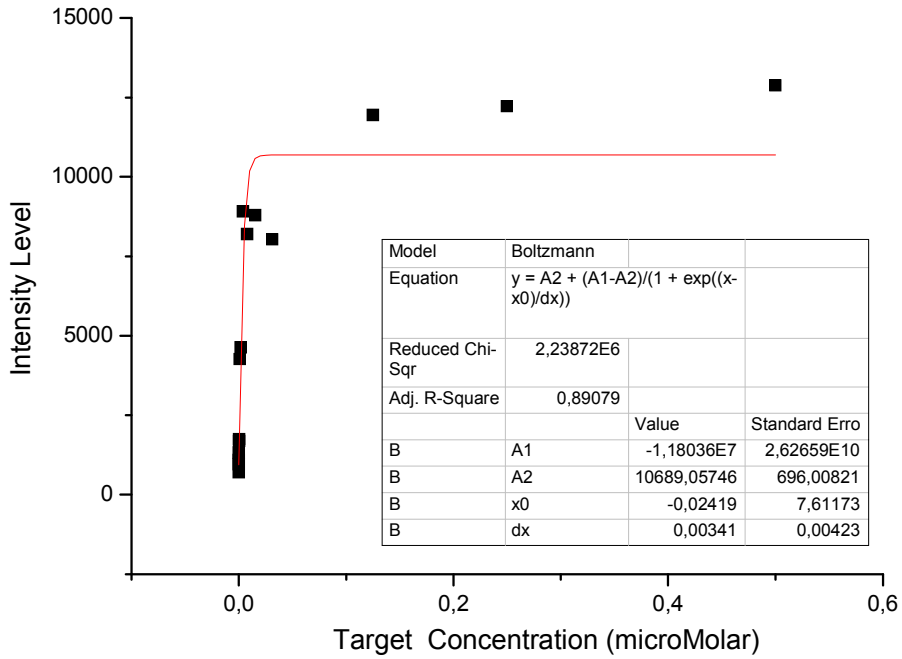
15000
10000
5000
0
Intensity Level
0,0
0,2
0,4
0,6
Target Concentration (microMolar)
Model Boltzmann
Equation y = A2 + (A1-A2)/(1 + exp((x-x0)/dx))
Reduced Chi-Sqr 2,23872E6
Adj. R-Square 0,89079
Value Standard Erro
B A1 -1,18036E7 2,62659E10
B A2 10689,05746 696,00821
B x0 -0,02419 7,61173
B dx 0,00341 0,00423

D

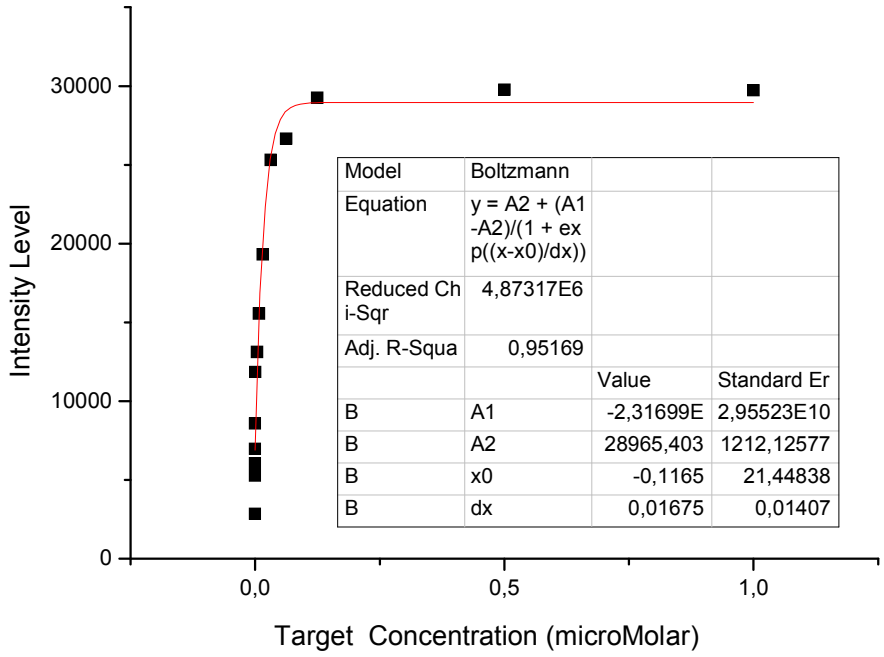
Intensity Level
30000
20000
10000
0
0,0
0,5
1,0
Target Concentration (microMolar)
Model Boltzmann
Equation y = A2 + (A1 -A2)/(1 + exp((x-x0)/dx))
Reduced Chi-Sqr 4,87317E6
Adj. R-Squa 0,95169
Value Standard Er
B A1 -2,31699E 2,95523E10
B A2 28965,403 1212,12577
B x0 -0,1165 21,44838
B dx 0,01675 0,01407

E

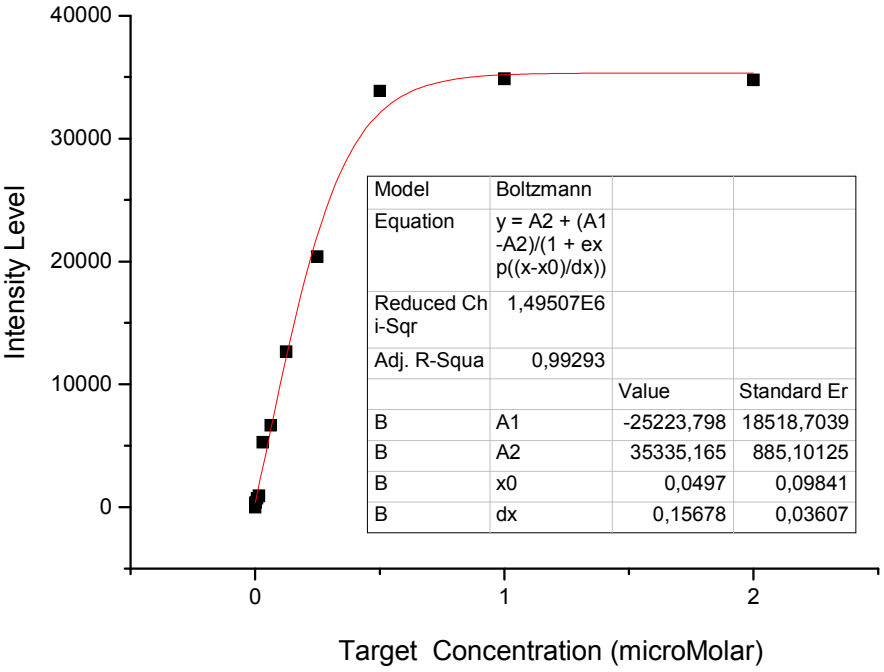
Intensity Level
40000
30000
20000
10000
0
0
1
2
Target Concentration (microMolar)
Model Boltzmann
Equation y = A2 + (A1 -A2)/(1 + exp((x-x0)/dx))
Reduced Chi-Sqr 1,49507E6
Adj. R-Squa 0,99293
Value Standard Er
B A1 -25223,798 18518,7039
B A2 35335,165 885,10125
B x0 0,0497 0,09841
B dx 0,15678 0,03607

F

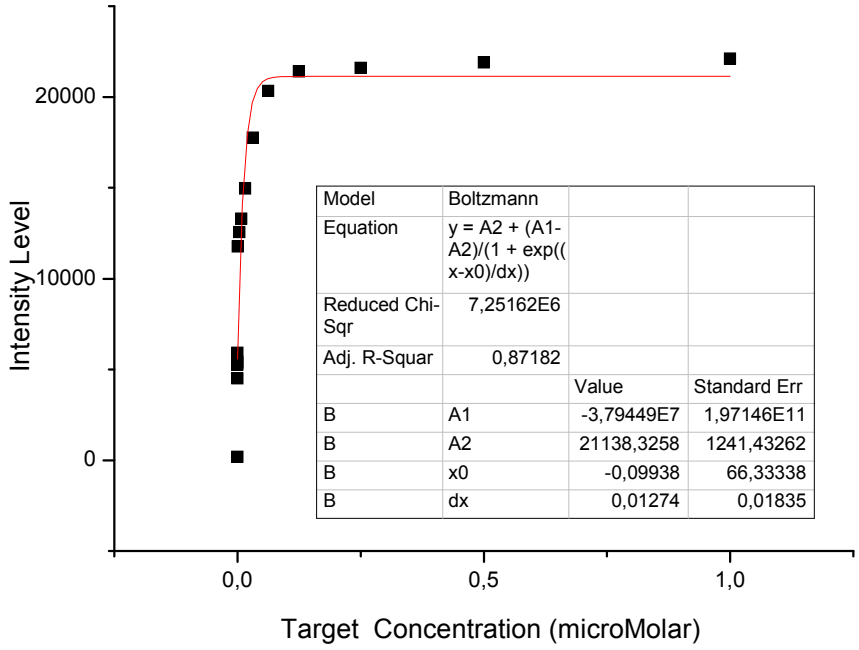

G

Fig 4.16. Boltzmann Regression Analysis of different Probe Oligonucleotide concentrations on *4X_MWNT_NHS* coated mercapto slide. **(A)** For Probe Oligonucleotide Concentration 2 mg/ml. **(B)** For Probe Oligonucleotide Concentration 1.5 mg/ml. **(C)** For Probe Oligonucleotide Concentration 1 mg/ml. **(D)** For Probe Oligonucleotide Concentration 0.75 mg/ml. **(E)** For Probe Oligonucleotide Concentration 0.5 mg/ml. **(F)** For Probe Oligonucleotide Concentration 0.25 mg/ml. **(G)** For Probe Oligonucleotide Concentration 0.125 mg/ml.

4.4 Characterization of MWNT Coated and Protein Immobilized Glass Slides

4.4.1 Scanning Electron Microscope

The *1/16X_MWNT_NHS* coated amine and *4X_MWNT_NHS* coated mercapto slide surfaces were examined with SEM **(Fig 4.17.)**. It must be mentioned that imaging of *1/16X_MWNT_NHS* coated amine slide was very hard as it is poorly conductive when compared to *4X_MWNT_NHS* coated mercapto slide. The lighter colored parts indicate the open functional groups ready for the protein or oligonucleotide attachment and they are clearly seen in all of the images.

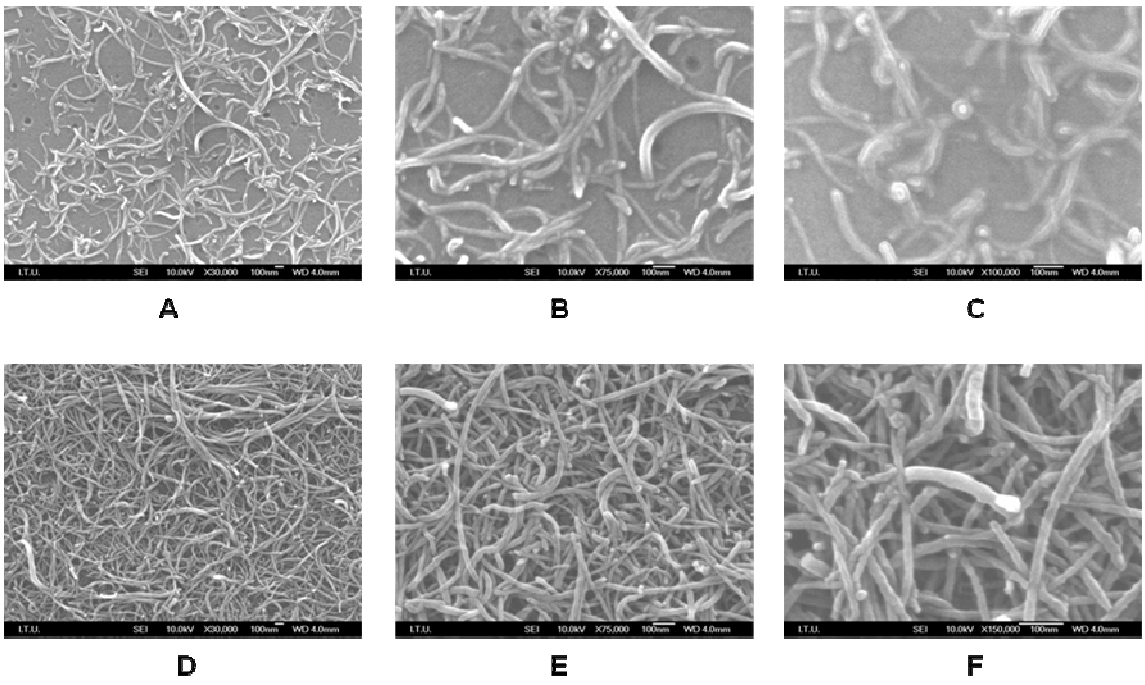

Fig 4.17. SEM images of *1/16X_MWNT_NHS* coated amine slide with different magnification factors **(A, B, C)** & SEM images of *4X_MWNT_NHS* coated mercapto slide with different magnification factors **(D, E, F).**

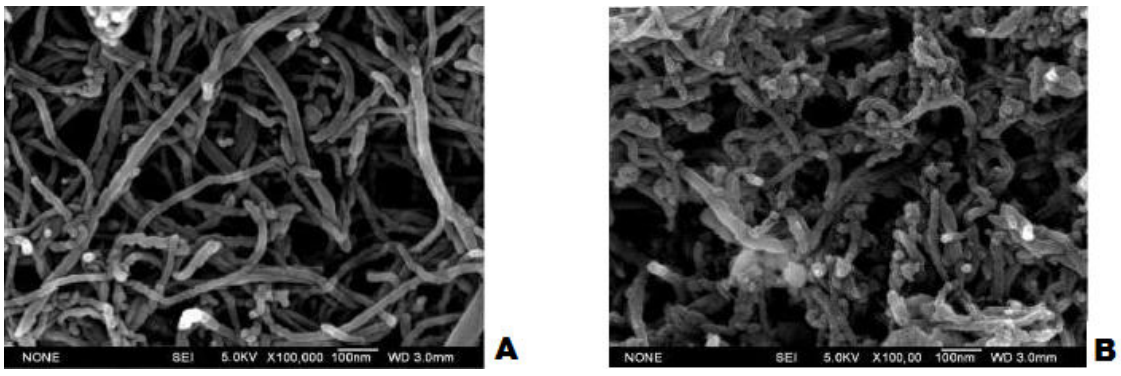

Fig 4.18. SEM images of *1/16X_MWNT_NHS* coated amine slide **(A)** & *4X_MWNT_NHS* coated amine slide **(B)**.

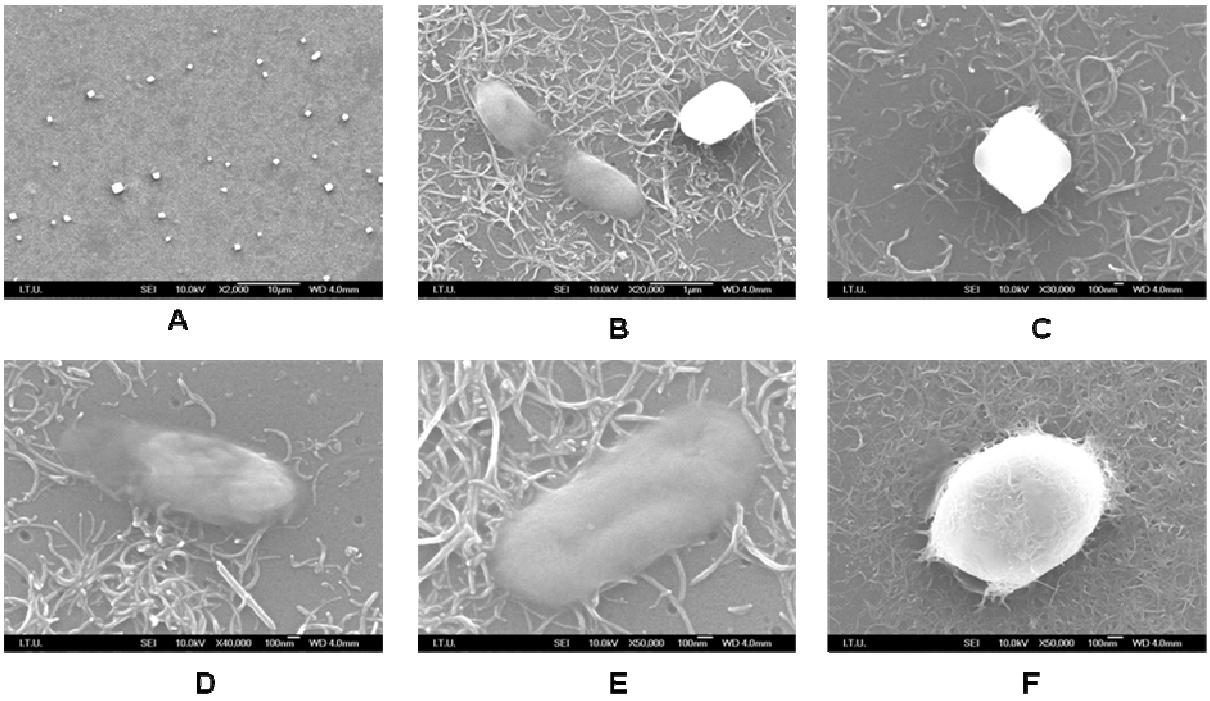

Fig 4.19. SEM images of immobilized proteins on *1/16X_MWNT_NHS* coated amine slide with different magnification factors.

In order to explain the signal reduction caused by higher MWNT_NHS concentrations on the surface, SEM analysis of *1/16X_MWNT_NHS* coated amine slide and *4X_MWNT_NHS* coated amine slide were performed **(Fig 4.18.)**. The dense structure observed in *4X_MWNT_NHS* coated amine slide presents thick MWNT_NHS coating on the surface blocking the sites on themselves for protein immobilization, therefore reducing the signal intensities. Protein immobilized surfaces are also examined with SEM. **Fig 4.19.** clearly shows the protein immobilization on *1/16X_MWNT_NHS* coated amine slide. It is also seen that MWNTs tied up the proteins which will result in enhancing their stability on the slide surface.

4.4.2 Atomic Force Microscopy

The *4X_MWNT_NHS* coated mercapto surface was examined with AFM before and after protein immobilization. **Fig 4.20.** indicates that the most of the MWNT_NHS are horizontally oriented on the surface, and their presence on the surface is clear with the undulating morphology. After protein immobilization, the height of the slide surface increases about 250nm indicating the presence of the proteins on the surface.

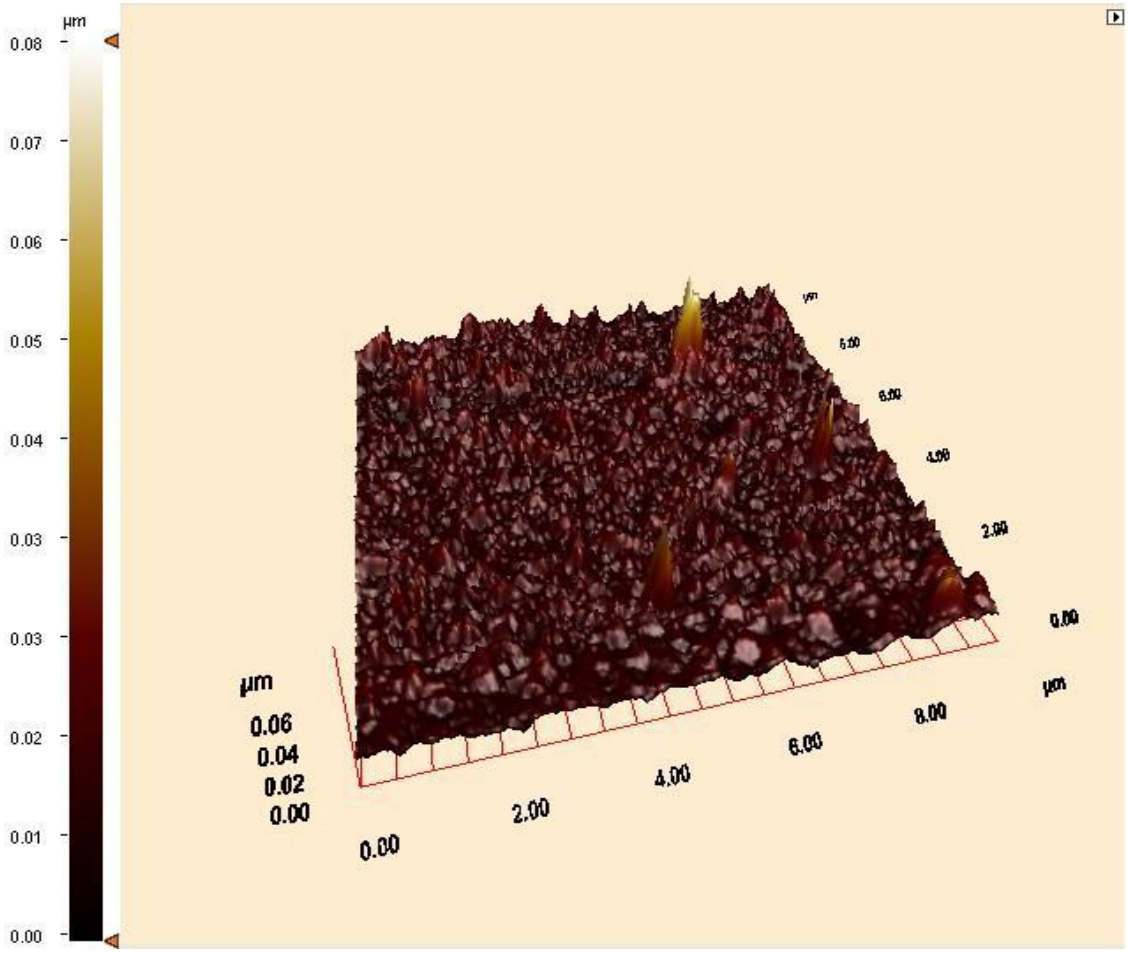

Fig 4.20. 3D- AFM image of *4X_MWNT_NHS* coated mercapto slide.

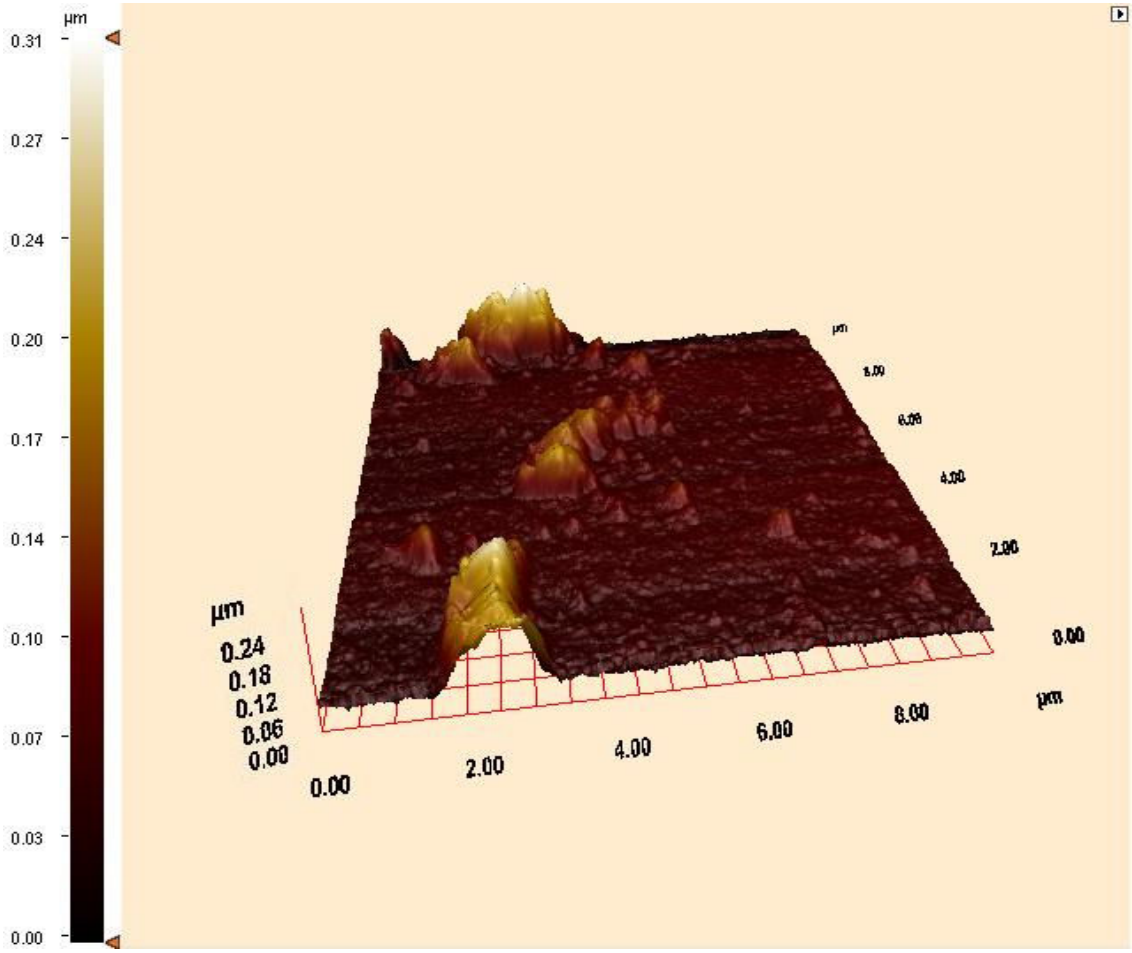

Fig 4.21. 3D- AFM image of *4X_MWNT_NHS* coated mercapto slide after protein immobilization.

5. DISCUSSION

Pristine carbon nanotubes were far away from being able to implement on application areas, firstly further chemical functionalizations were needed to achieve their dispersion in organic and inorganic solvents. Successful dispersion of the MWNTs was achieved with sonication and addition of Triton X-100 as a dispersant in every step. The applied covalent functionalization strategies in this work were examined and characterized with DLS, FTIR and SEM experiments. All of the characterization methods proposed EDC/NHS treatment of carboxyl functionalized MWNTs as the best functionalization process with the highest yield for chemical functionalization and best capability of protein binding among all. APTES modified MWNT_OH were not chosen for further experiments considering their low chemical functionalization yield and poor dispersion in aqueous solvents related to the high surface interaction between the APTES modified MWNTs. Also, MWNT_COOH purchased from Arry Nanotechnologies were preferred to carboxyl functionalized Baytubes® with the same reason of higher yield for chemical functionalization. This can be due to the low efficiency in carboxyl functionalization process of Baytubes® which can be further optimized by changing the sonication period and incubation temperature. Protein immobilization on MWNT_NHS is successfully achieved via EDC/NHS treatment of carboxyl functionalized MWNTs, as mentioned below and analyzed via SEM, where immobilized proteins on the surface of MWNT_NHS are clearly seen.

Next steps involved implementation of MWNT_NHS as new microarray substrates. After the microarray experiments which are planned on MWNT_NHS coated slides with different functional groups on them, *1/16X_MWNT_NHS* coated amine slide and *4X_MWNT_NHS* coated mercapto slide were chosen for further antibody array experiments where *1X_MWNT_NHS* amine slide and *4X_MWNT_*NHS coated mercapto slide were chosen for oligonucleotide array experiments. Performed experiments showed the signal enhancement effects of MWNT_NHS on surface both for antibody and oligonucleotide arrays. These signal enhancements supports the hypothesis of this study which is making use of carbon nanotube properties like high binding capacity of them for biomolecules without changing their biologically active conformation and their low auto fluorescence, generating a high signal to noise ratio. The risk by the use of a 3D surface instead of a 2D could be the loss of fluorescence intensity in the depth of the

surface structure. However, the results show that the depth fluorescence photons were coming from was in conformation with the standard depth of focus of commercial fluorescence scanner. A sigmoidal intensity increase as a function of fluorescent protein and oligonucleotide concentration was noticed for the MWNT substrate.

The characterization of the MWNT_NHS coated and protein immobilizied slides were also achieved via SEM and AFM analysis. The results confirm the efficient MWNT_NHS coating of the slide surfaces and presents the efficient protein immobilization on the surface of MWNT coated slides. To sum up, MWNT coated slides appeared to be good candidates as new substrates for antibody and oligonucleotide arrays after all the characterization experiments.

6. CONCLUSION & FUTURE REMARKS

This work includes a method of MWNT implementation for optical biosensor platforms. Covalent carbodiimide-activated amidation of the MWNTs were chosen as the best functionalization method for biomolecule immobilization. The characterization techniques confirmed the successful functionalization of MWNTs as well as the successful immobilization of biomolecules on the functionalized MWNT surfaces. Microarray experiments, in which MWNT_NHS was proposed as a new microarray substrate, were performed in order to characterize the dynamic range of immobilized probe biomolecules. Results of the designed microarray experiments suggest MWNTs as good candidates for optical sensor platforms combining the benefits of high binding capacity of MWNTs for biomolecules without changing their biologically active conformation, increased surface area of 3D carbon nanotube structures, and the excellent low auto fluorescence of MWNTs generating a high signal to noise ratio.

The unique physical and mechanical properties of carbon nanotubes make them ideal candidates for electroanalytical studies. Their enhanced active surface area, the anti-fouling capability of the modified surfaces and the electro catalytic ability promise their successful implementation also in other biosensing transducers, in addition to the optical systems which this work mainly focuses on. Therefore, future work includes implementation of functionalized MWNTs as a surface for capacitive biosensors. In addition to the enhancement effects of MWNTs suggested in this study for optical systems, their electro catalytic ability promise for their enhancements also in the capacitive biosensor platform which is being investigated in our laboratory.

APPENDIX A

Data Sheets of Carbon Nanotubes

baytubes® C 150 P

Product Specifications

Property	Value	Unit	Method
C-Purity	> 95	%	Elementary analysis
Free amorphous carbon	Not detectable	%	TEM
Number of walls	3-15	-	TEM
Outer mean diameter	13-16	nm	TEM
Outer diameter distribution	5-20	nm	TEM
Inner mean diameter	4	nm	TEM
Inner diameter distribution	2-6	nm	TEM
Length	1 - >10	µm	SEM
Bulk density	140-160	kg/m³	EN ISO 60
Loose agglomerate size	0,1-1	mm	PSD

ARRY®

Nano Materials and Nanotechnology

Stock number	-OH -COOH	Diameter	Purity	Length	Ash	SSA
ARQM003	-OH content: 1~7wt%	10-20nm	>95wt%	＜20μm	<1.5wt%	>220 m^2/g
ARSM003	-COOH content: 1~6wt%	10-20nm	>95wt%	＜20μm	<1.5wt%	>200 m^2/g

APPENDIX B

Data Sheets of Antibodies & Antigens

Monoclonal Antibody Data Sheet

Product:	C-Reactive Protein (C-RP)		
Catalog #:	**10-C33A**	**Host :**	mouse
Immunogen:	Highly pure immuno grade C-RP		
Clone #:	M701289	**Batch #:**	901
Subclass:	IgG1		
Concentration:	4.9mg/ml	**Affinity Constant:**	~1.1 x 1010 L/M
Cross Reactivity:	Specific for C-RP only. No cross reaction with other serum proteins		
Form:	Purified by Protein A, supplied in PBS buffer with 0.1% NaN3		
Storage:	4oC short term only, for routine storage, aliquot and freeze at -20oC		
Additional Remarks:	Use as the capture antibody matched with Cat# 10-C33C clone M701289 as the detection antibody.		

E-mail: antibodies@fitzgerald-fii.com

Antigen Data Sheet

Product: ***C-Reactive Protein (C-RP) Highly Pure***

Catalog #: 30-AC05

New Catalog #: 30-AC05

Grade: High Purity

Purity: >95% (Iodination grade) by SDS-PAGE and IEP

Source: human fluids

Concentration: 2.94mg/ml by RID using CAP/IFCC control

Contaminants: none, single band determined by SDS PAGE, and Immunoelectrophoresis.

Form: Liquid, in 100 mM Tris, 200 mM NaCl, pH 7.5 with 2 mM $CaCl_2$ and 0.1% NaN_3

Biohazard: Raw material tested and found non-reactive for anti-HIV 1/2 , anti-HCV and HBsAg by FDA approved methods.

Storage: 4ºC short term, -20ºC long term

Additional Remarks: C-RP Antigen can be used for labeling or immunogen purposes.

Monoclonal Antibody Data Sheet

Product:	C-Reactive Protein (C-RP)		
Catalog #:	**10-C33C**	**Host :**	mouse
Immunogen:	Highly pure immuno grade C-RP		
Clone #:	M701288	**Batch #:**	1710
Subclass:	IgG_{2a}		
Concentration:	4.35mg/ml	**Affinity Constant:**	~1.0 x 10^10 L/M
Cross Reactivity:	Specific for C-RP only. No cross reaction with other serum proteins		
Form:	Protein A purified, supplied in PBS buffer, pH 7.3, with 0.9% NaCl, and 0.1% Na Azide		
Storage:	4˚C or -20˚C for long term storage.		
Additional Remarks:	Recommended use: as the conjugate/ label, matched with Cat# 10-C33A clone M701289 as the solid phase.		

7. REFERENCES

[1]. L.C. Clark and C. Lyons, Electrode Systems for Continuous Monitoring in Cardiovascular Surgery, *Annals of the New York Academy of Sciences 102* pp. 29-45, (1962).

[2]. T.-R. Hsu, *MEMS & Microsystems: Design and Manufacture,* McGraw-Hill, Boston, MA; pp. 39-40, (2002).

[3]. Sauerbrey GZ. Use of quartz crystal vibrator for weighting thin films on a microbalance. *Phys*; 155:206–22, (1959).

[4]. T.-R. Hsu, *MEMS & Microsystems: Design and Manufacture,* McGraw-Hill, Boston, MA; pp. 47, (2002).

[5]. T.-R. Hsu, *MEMS & Microsystems: Design and Manufacture,* McGraw-Hill, Boston, MA; pp. 40-41, (2002).

[6]. MV Pishko and SH Kim, "Practical Approaches to Biosensors," presentation at a BioDot workshop at Penn State University (State College, PA), October 26, (2006).

[7]. M. Sequeira, M. Bowden, E. Minogue, D. Diamond. *Talanta* 56, 355–363, (2002).

[8]. H. Suzuki. *Mater. Sci. Eng. C* 12, 55–61, (2000).

[9]. L. Tiefenauer and R. Ros. *Colloids Surf. B: Biointerfaces* 23, 95–114, (2002).

[10]. S. Kossek, C. Padeste, L. X. Tiefenauer, H. Siegenthaler. *Biosens. Bioelectron.* 13, 31–43, (1998).

[11]. Ekins RP. *J. Pharm. Biomed. Anal.*; 7: 155, (1989).

[12]. Watson A, Mazumder A, Stewart M, Balasubramanian S. *Curr. Opin. Biotechnol.*; 9: 609, (1998).

[13]. Chaudhuri JD. *Med. Sci. Monit.*; 11: RA52, (2005).

[14]. Templin MF, Stoll D, Schrenk M, Traub PC, Vohringer CF, Joos TO. *Trends Biotechnol.*; 20: 160, (2002).

[15]. Kodadek T. *Chem. Biol.*; 8: 105, (2001).

[16]. Ziauddin J, Sabatini DM. *Nature*; 411: 107, (2001).

[17]. Breslauer DN, Lee PJ, Lee LP. *Mol. Biosyst*; 2: 97, (2006).

[18]. Heller MJ. *Annu. Rev. Biomed. Eng.*; 4: 129, (2002).

[19]. van Hal NLW, Vorst O, van Houwelingen AMML, Kok EJ, Peijnenburg A, Aharoni A, van Tunen AJ, Keijer J. *J. Biotechnol.*; 78: 271, (2000).

[20]. Mitchell P. A perspective on protein microarrays. *Nat Biotechnol*. 20(3):225-9, (2002).

[21]. Haab BB, Dunham MJ, Brown PO. *Genome Biology* 2, 0004.1-0004.13, (2001).

[22]. Lofas S, Johnsson B, Tegendahl K, Ronnberg I. *J. Colloid Interface Sci.* 65, 423-431, (1993).

[23]. Afanassiev V, Hanemann V, Wolf S. *Nucleic Acids Res.* 28: 12, e66, (2002).

[24]. T.O. Joos, M. Schrenk, P. Hopfl, K. Kroger, U. Chowdhury, D. Stoll, D. Schorner, M. Durr, K. Herick, S. Rupp *et al*. *Electrophoresis*. 21, pp. 2641–2650, (2000).

[25]. H. Ge. *Nucleic Acids Res*. 28, (2000).

[26]. R.M. De Wildt, C.R. Mundy, B.D. Gorick and I.M. Tomlinson. *Nat. Biotechnol.* 18, pp. 989–994, (2000).

[27]. MacBeath, G. and S.L. Schreiber. Printing proteins as microarrays for high-throughput function determination. *Science 289*:1760-1763, (2000).

[28]. H Zhu, JF Klemic, S Chang, P Bertone, A Casamayor, KG Klemic, D Smith, M Gerstein, MA Reed and M Snyder. *Nat Genet* 26, pp. 283–289, (2000).

[29]. G. MacBeath, A.N. Koehler and S.L. Schreiber. *J. Am. Chem. Soc.* 121, pp. 7967–7968, (1999).

[30]. S. Heyse, H. Vogel, M. Sanger and H. Sigrist. *Protein Sci.* 4, pp. 2532–2544, (1995).

[31]. Terrones, M. *Annual Review of Materials Research.* 33: p. 419-501, (2003).

[32]. Ouyang, M., J.-L. Huang, and C.M. Lieber. *Annual Review of Physical Chemistry.* 53: p. 201-220. 13, (2002).

[33]. Zhou, O., et al. *Accounts of Chemical Research*. 35(12): p. 1045-1053, (2002).

[34]. Gooding, J.J. *Electrochimica Acta*. 50(15): p. 3049-3060, (2005).

[35]. Rao, C.N.R., A. Müller, and A.K. Cheetham, *The Chemistry of Nanomaterials*. Weinheim: WILEY-VCH Verlag GmbH & Co. KgaA, (2004).

[36]. Popov, V.N., "Carbon nanotubes: properties and applications", *Materials Science and Engineering Reports*, Vol 43, 61-102, (2004).

[37]. T. Guo, P. Nikolaev, A.G. Rinzler, D. Tomanek, D.T. Colbert and R.E. Smalley, *J. Phys. Chem*. 99, 10694, (1995).

[38]. Yacaman, M. et al., "Catalytic growth of carbon microtubules with fullerene structure", *Applied Physics Letters*, Vol 62, 202-204, (1993).

[39]. Ivanov, V. et al., "The study of carbon nanotubes produced by catalytic method", *Chemical Physics Letters*, Vol 223, 329, (1994).

[40]. Amelinckx, S. et al., "A formation mechanism for catalytically grown helix shaped graphite nanotubes", *Science*, Vol 265, 635, (1994).

[41]. Hou, P. Liu C. Cheng H. Purification of carbon nanotubes. (2003).

[42]. Liang, W. J., Bockrath, M., Bozovic, D., Hafner, J. H., Tinkham, M., and Park, H. *Nature* 411 (6838), 665-669, (2001).

[43]. Lide, D. R., ed., Electrical resistivity of pure metals, in *CRC Handbook of Chemistry and Physics, 88th Edition (Internet Version),* CRC Press/Taylor and Francis, Boca Raton, FL, pp. 12-39 -12-40, (2008).

[44]. Ebbesen, T. W. and Ajayan, P.M. *Nature* 358, 220-222 (1992).

[45]. Mattia, D., Rossi, D., M. P., Kim, B. M., Korneva, G., Bau, H. H., and Gogotsi, Y. *Journal of Physical Chemistry B* 110 (20), 9850- 9855 (2006).

[46]. Wong, E. W., Sheehan, P. E., and Lieber, C. M. *Science* 271, 1971-1974 (1997).

[47]. Lee, S.B., R. Koepsel, D.B. Stolz, H.E. Warriner and A.J. Russell, *J. Am. Chem. Soc.* 126, p. 13400. C.F., (2004).

[48]. Lopez, S.O. Nielsen, P.B. Moore and M.L. Klein, *Proc. Natl. Acad. Sci.* 101, p. 4431, (2004).

[49]. Hone, J., Whitney, M., Zettl, A., *Synth. Met*. 103, 2498, (1999).

[50]. Unger, E., Graham, A., Kreupl, F., Liebau M., Hoenlein, W., *Curr. Appl. Phys*. 2, 107,(2002).

[51]. Chen, W., Tao, X., Xue, P., Cheng, X., *Appl. Surf. Sci*. 252, 1404, (2005).

[52]. Zhao, B., H. Hu, and R.C. Haddon. *Advanced Functional Materials*. 14(1): p. 71-76, (2004).

[53]. Hamon, M.A., et al., *Advanced Materials* (Weinheim, Germany). 11(10): p. 834-840, (1999).

[54]. Pompeo, F. and D.E. Resasco. *Nano Letters*. 2(4): p. 369-373, (2002).

[55]. Chen, J., et al., *Journal of Physical Chemistry B*. 105(13): p. 2525-2528, (2001).

[56]. Kahn, M.G.C., S. Banerjee, and S.S. Wong. *Nano Letters*. 2(11): p. 1215-1218, (2002).

[57]. Chattopadhyay, D., I. Galeska, and F. Papadimitrakopoulos. *Journal of the American Chemical Society*. 125(11): p. 3370-3375, (2003).

[58]. Sun, Y., S.R. Wilson, and D.I. Schuster. *Journal of the American Chemical Society*. 123(22): p. 5348-5349, (2001).

[59]. Chen, J., et al., *Science* (Washington, D. C.). 282(5386): p. 95-98, (1998).

[60]. Hamon, M.A., et al., *Applied Physics A: Materials Science & Processing*, 74(3): p. 333-338, (2002).

[61]. Alvaro, M., et al., *Journal of Physical Chemistry B*, 109(16): p. 7692-7697, (2005).

[62]. Frackowiak E, Jurewicz K, Delpeux S, Beguin F. *NATO Science Series, II: Mathematics, Physics and Chemistry* 91: 305, (2003).

[63]. Sherigara B S, Kutner W, D'Souza F. *Electroanalysis* 15: 753, (2003).

[64]. Bianco A, Kostarelos K, Partidos C D, Prato M. *Chem Commun* 5: 571, (2005)

[65]. Katz E, Willner I. *Chem Phys Chem 5*: 1084, (2004).

[66]. Star, A.; Stoddart, J. F.; Steuerman, D.; Diehl, M.; Boukai, A.; Wong, E. W.; Yang, X.; Chung, S.-W.; Choi, H.; Heath, J. R. Angew. *Chem., Int. Ed. Engl*. 40, 1721- 1725, (2001).

[67]. Ajayan, P. M.; Zhou, O. Z. Applications of carbon nanotubes. *Top. Appl. Phys*., 80, 391-425, (2001).

[68]. Tsang, S. C.; Guo, Z.; Chen, Y. K.; Green, M. L. H.; Hill, H. A. O.; Hambley, T. W.; Sadler, P. J. *Angew. Chem., Int. Ed. Engl*. 36, 2198-2200, (1997).

[69]. Balavoine, F.; Schultz, P.; Richard, C.; Mallouh, V.; Ebbesen, T. W.; Mioskowski, C. *Angew. Chem., Int. Ed. Engl*. 38, 1912-1915, (1999).

[70]. Mattson, M. P.; Haddon, R. C.; Rao, A. M. *J. Mol. Neurosci*. 14, 175-182, (2000).

[71]. Huang, W.; Taylor, S.; Fu, K.; Lin, Y.; Zhang, D.; Hanks, T. W.; Rao, A. M.; Sun, Y.-P. *Nano Lett.*, 2, 311-314, (2002).

[72]. P. Avouris, Carbon Nanotube Electronics, *Chemical Physics 281* pp. 429- 445, (2002).

[73]. P. Avouris, Carbon Nanotube Electronics and Optoelectronics, *Mrs Bulletin 29* pp. 403-410, (2004).

[74]. R.H. Baughman, A.A. Zakhidov, and W.A. de Heer. *Science 297* pp. 787-792, (2002).

[75]. J. Okuno, K. Maehashi, K. Kerman, Y. Takamura, K. Matsumoto, E. Tamiya, *Biosens. Bioelectron*. 22 2377, (2007).

[76]. C. Ou, R. Yuan, Y. Chai, M. Tang, R. Chai, X. He, *Anal. Chim. Acta* 603 205, (2007).

[77]. S. Viswanathan, L. Wu, M.-R. Huang, J.A. Ho, *Anal. Chem.* 78 1115, (2006).

[78]. V. Cataldo, A. Vaze, J.F. Rusling, *Electroanalysis* 20, 115, (2008).

[79]. Y.H. Yun, A. Bange, W.R. Heineman, H.B. Halsall, V.N. Shanov, Z. Dong, S. Pixley, M. Behbehani, A. Jazieh, Y. Tue, D.K.Y. Wong, A. Bhattacharya, M.J. Schulz, *Sens. Actuators B* 123, 177, (2007).

[80]. Z. Wang, S. Xiao, Y. Chen, *Electroanalysis* 17, 2057, (2005).

[81]. Y. Ye, H. Ju, *Biosens. Bioelectron*. 21, 735, (2005).

[82]. K. Kerman, Y. Morita, Y. Takamura, E. Tamiya, *Anal. Bioanal. Chem*. 381, 1114, (2005).

[83]. A. Erdem, P. Papakonstantinou, H. Murphy, *Anal. Chem*. 78, 6656, (2006).

[84]. J. Li, Q. Liu, Y. Liu, S. Liu, S. Yao, *Anal. Biochem*. 346, 107, (2005).

[85]. Y. Xu, X. Ye, L. Yang, P. He, Y. Fang, *Electroanalysis* 18, 1471, (2006).

[86]. H. Qi, X. Li, P. Chen, C. Zhang, *Talanta* 72, 1030, (2007).

[87]. Z. Chang, H. Fan, K. Zhao, M. Chen, P. He, Y. Fang, *Electroanalysis* 20, 131, (2008).

[88]. Zhu, H. and Snyder, M. Protein chip technology. *Current Opinion in Chemical Biology*, 7:55-63, (2003).

[89]. Merkoci, A., Carbon nanotubes in analytical sciences. *Microchimica Acta*, 152(3-4): p. 157-174, (2006).

[90]. Richa Rastogi, Rahul Kaushal, S.K. Tripathi, Amit L. Sharma, Inderpreet Kaur, and Lalit M. Bharadwaj., *Journal of Colloid and Interface Science* Volume 328, Issue 2, pp: 421-428, (2008).

[91]. Weijie Huang, Yi Lin, Shelby Taylor, Jay Gaillard, Apparao M. Rao, and Ya-Ping Sun. *NANO LETTERS* 2002 Vol. 2, No. 3, 231-234, (2002).

[92]. A.R. Boccaccini, D.R. Acevedo, G. Brusatin and P. Colombo, *J Eur Ceram Soc* 25, p. 1515, (2005).

[93]. Dovbeshko, G. I., Chegel, V. I., Gridina, N. Y., Repnytska, O. P., Shirshov, Y. M., Tryndiak, V. P., Todor, I. M. and Solyanik, G. I. *Biopolymer (Biospectroscopy)* 67, pp. 470-486, (2002).

[94]. Dovbeshko, G. I., Gridina, N. Y., Kruglova, E. B. and Pashchuk, O. P. *Talanta* 53, pp. 233-246, (1997).

[95]. Fung, M. F. K., Senterman, M. K., Mikhael, N. Z., Lacelle, S. and Wong, P. T. T. *Biospectroscopy* 2, pp. 155-165, (1996).

[96]. Gazi, E., Dwyer, J., Gardner, P., Ghanbari-Siakhani, A., Wde, A. P., Lockyer, N. P., Vickerman, J. C., Clarke, N. W., Shanks, J. H., Scott, L. J., Hart, C. A. and Brown, M. *Journal of Pathology* 201, pp. 99-108, (2003).

[97]. Farguharson, S., Shende, C., Inscore, F. E., Maksymiuk, P. and Gift, A. *Journal of Raman Spectroscopy* 36, pp. 208-212, (2005).

[98]. Schulz, H. and Baranska, M. *Vibrational Spectroscopy* 43, pp.13-25, (2007).